J. Fluid Mech. (1986), *vol.* 172, *pp.* 93–126
Printed in Great Britain

The structure of a chemically reacting plane mixing layer

By S. M. MASUTANI† AND C. T. BOWMAN
Department of Mechanical Engineering, Stanford University, Stanford, CA 94305, USA

(Received 30 July 1985 and in revised form 1 April 1986)

Experiments were performed to examine the structure of a chemically reacting, gas-phase, two-stream plane mixing layer. Temporally and spatially resolved measurements of streamwise velocity and of the concentrations of a reactant and product species and a conserved scalar were recorded across the mixing layer at streamwise locations between $Re_\delta = 730$–2520. Non-reacting flow experiments were conducted to establish the entrainment and mixing characteristics of the layer. Reacting flow experiments were performed using dilute concentrations of the reactants, NO and O_3, to ensure that the flow field remained isothermal. The probability density functions (p.d.f.s) and associated statistical quantities of the conserved and reactive scalars are compared with results from previous analytical and experimental studies. The data suggest, in concert with the Broadwell–Breidenthal model, that fluid in the mixing layer exists in three states: tongues of unmixed free-stream fluid which, on occasion, stretch across the layer; finite-thickness interfacial diffusion zones of mixed fluid which border the parcels of unmixed fluid; and regions comprising fluid of nearly homogeneous composition. The data also confirm previously reported asymmetry in entrainment rates from the two feed streams and show the important role of molecular diffusion in the mixing process. A fast-chemistry assumption, applied to predict reactive-species concentrations from the measured conserved-scalar p.d.f.s, overestimates the extent of reaction, indicating the importance of finite-rate chemistry for the present conditions. A Damköhler number, based on large-scale mixing times, is shown to be useful in determining the applicability of a fast-chemistry analysis to reacting mixing layers.

1. Introduction

Chemically reacting mixing layers represent a technologically important class of flows, which includes chemical and biological processing systems and combustion devices. Because of their importance, these flows have been the subject of extensive experimental and theoretical study. In spite of this effort, the understanding of mixing and chemical reaction in these flows is incomplete, as evidenced by discrepancies between experimental observations and predictions from current turbulent reacting flow models (Driscoll, Schefer & Dibble 1984; Koochesfahani & Dimotakis 1984; Masutani 1985). The principal objectives of the present study were to obtain experimental data on the concentration fields of both reactive and conserved scalars (i.e. reactant, product and conserved species) in a well-characterized, chemically reacting mixing layer, and to use these data to infer flow-field structure and to determine processes important in entrainment, mixing and subsequent reaction of

† Present address: Hitachi Research Laboratory, Ibaraki-ken, Japan.

initially unmixed reactants. In addition, these measurements would supplement the existing data base for testing new and existing models of turbulent reacting flows.

The flow configuration examined was a gas-phase, two-stream, plane mixing layer, in which each stream contained a single reactant species. The plane mixing layer was selected because it is representative of the mixing and reaction zones that exist in real combustion devices, while affording a certain degree of experimental simplicity. Unlike the mixing zones in a round jet, the flow field in a plane mixing layer may be nearly two-dimensional in certain situations, allowing application of line-of-sight optical diagnostic techniques. A binary reaction that occurs rapidly and irreversibly in dilute concentrations was selected for study. Such a reaction ensured isothermal (constant-density) flow conditions and allowed isolation of the effects of mixing on the reaction process. In the present investigation, the two reactants were nitric oxide and ozone. An additional feature of this reaction is that both reactant and product species may be measured by available optical techniques.

The structure of non-reacting plane mixing layers has been examined in numerous experimental studies (e.g. Brown & Roshko 1974; Winant & Browand 1974; Konrad 1976; Bates 1977; Lasheras, Cho & Maxworthy 1986), and there have been a limited number of studies of reacting plane mixing layers in liquids (Breidenthal 1981; Koochesfahani 1984; Lasheras *et al.* 1986) and in gases (Alber & Batt 1976; Batt 1977; Wallace 1981; Mungal 1983). While these studies have accomplished much in the way of establishing the structure and fundamental entrainment and mixing processes in the plane mixing region, there is a noticeable lack of experimental data on scalar transport and reaction in gas-phase flows in the regime immediately prior to the mixing transition, i.e. prior to the streamwise location at which a significant increase in mixing has been observed (Konrad 1976; Breidenthal 1981; Koochesfahani 1984). The significant differences that exist between concentration data obtained in liquid and gaseous flows at similar Reynolds numbers suggest that molecular diffusion plays an important role in establishing the concentration structure of reacting gas-phase mixing layers. The influence of these diffusion processes on the concentration field may be particularly pronounced in pre-mixing transition flows. Because the mixing zones that occur immediately downstream from fuel injectors in many practical combustion devices often may be represented by pre-mixing transition flows, the importance of determining the properties of the layer in this flow regime, with regard to characteristics such as ignition and flame stabilization, is evident.

The present investigation provides information on the concentration structure and data on the dynamical variables of a gas-phase, pre-mixing transition mixing layer, under both non-reacting and reacting flow conditions. The non-reacting flow experiments were conducted to establish the hydrodynamic field and the entrainment and mixing characteristics of the mixing layer. Since the reacting flow was isothermal, the non-reacting flow results can be used in the interpretation of the reacting flow experiments.

2. Experimental facility

Experiments were conducted in an atmospheric-pressure, continuous flow, open-circuit wind-tunnel facility in which NO and O_3 were introduced into N_2 carrier gas (figure 1). The facility was designed to allow independent variation of free-stream velocities and reactant concentrations. With the current gas supply system, velocities of up to 20 m/s are possible. For the present experiments, the free-stream velocities were set at 6 and 3 m/s. A detailed description of the facility has been presented by Masutani (1985).

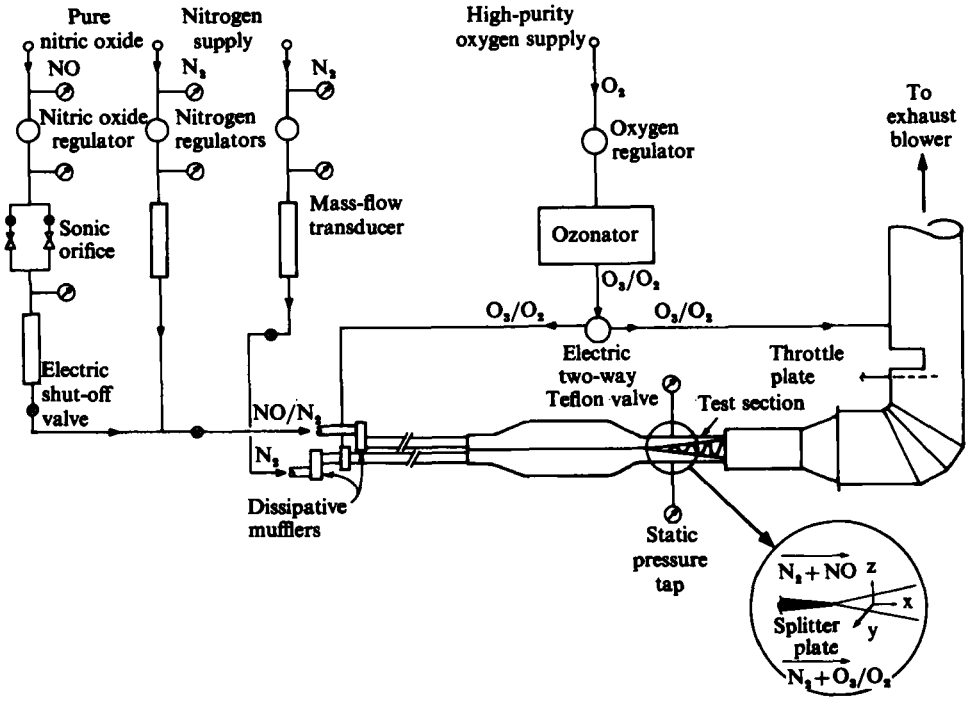

FIGURE 1. Schematic diagram of the mixing-layer facility.

The N_2 carrier-gas flows are metered by high-accuracy pressure regulators, and the flow rates are measured by linear mass-flow transducers. The reactant species, NO and O_3, are injected into the carrier gas some distance upstream from the test section to ensure complete mixing. The NO is supplied from a bank of gas cylinders containing pure (98.5 % minimum purity) nitric oxide. The NO flow rate is controlled and measured using a system similar to the N_2 supply. An ozonator provides a continuous supply of O_3. Gas leaving the ozonator consists of a mixture of O_3 and O_2. Under typical operating conditions, approximately 3 % of the mixture by mass is O_3. The O_3/O_2 mixture passes through a Teflon tube into an annular injection manifold mounted on one of the N_2 supply lines. The interior surface of this supply line is Teflon coated to reduce surface decomposition of O_3.

Dissipative mufflers are mounted in the supply lines to reduce acoustic perturbations to the flow. Long run-in sections ensure that fully developed pipe-flow velocity distributions exist at the inlets to the tunnel. The flow issuing from the run-in sections passes through perforated plates and screens prior to expansion in a wide-angle diffuser. Flow separation is avoided by mounting low-solidity perforated plates across the inlet, exit and midpoint of the diffuser. The flow subsequently enters a constant-area plenum and passes through a length of honeycomb and four low-solidity screens. A two-dimensional nozzle, with a 2.8:1 contraction ratio, accelerates the gas prior to entering the test section. The two initially separate gas streams meet at the trailing edge of a Teflon-coated brass splitter plate, which extends approximately 2 mm beyond the exit plane of the nozzle. The splitter plate is tapered on both sides (5° enclosed angle) and terminates in an edge with a thickness of ≈ 0.1 mm.

Mixing of the two streams and subsequent chemical reaction occur in an enclosed 4 cm high × 10 cm wide × 20 cm long test section. The sidewalls of the test section are

0.635 cm thick fused-quartz windows which allow optical access for flow visualization. The top and bottom test-section walls are adjustable, permitting variation of the streamwise pressure gradient. In all of the experiments reported here, the walls were adjusted to give a zero streamwise pressure gradient.

3. Measurement techniques

A principal objective of the present study was acquisition of temporally and spatially resolved measurements of the concentrations of a reactant and a product species and of a conserved scalar in the mixing layer. The species of interest in the $NO + O_3$ system are the reactants and products shown below in the complete reaction mechanism:

$$NO + O_3 \rightarrow NO_2 + O_2, \tag{3.1a}$$

$$NO + O_3 \rightarrow NO_2^* + O_2, \tag{3.1b}$$

$$NO_2^* + M \rightarrow NO_2 + M, \tag{3.1c}$$

$$NO_2^* \rightarrow NO_2 + h\nu, \tag{3.1d}$$

$$NO + NO + O_2 \rightarrow 2\,NO_2, \tag{3.1e}$$

where NO_2^* is electronically excited nitrogen dioxide, which decays via chemiluminescent emission of radiation and by collisional de-excitation. Kinetics calculations for the present experimental conditions indicate that (3.1*a*) is the dominant reaction path, with approximately 93% of the NO_2 produced going directly to the ground state. The species that are candidates for optical measurement are the reactant species, NO and O_3, and the product species, NO_2. Since O_2 exists both before chemical reaction (as a component of the O_3-bearing feed stream) and after (as a product), variation in O_2 concentration is not a sensitive measure of reaction.

In the present study, O_3 and NO_2 were measured using absorption spectroscopy. The diagnostic employed in these measurements was a fibre-optic absorption probe. This probe has been described in detail in Masutani & Bowman (1982). The probe system, shown in figure 2, simultaneously monitors absorption at two wavelengths, 253.7 nm and 435.8 nm (emission lines of the mercury lamp), corresponding to absorption by O_3 and NO_2 respectively. Reference intensities I_0 at the two wavelengths are obtained by diverting a portion of the lamp output onto a set of reference detectors. A Lambert–Beer-type absorption relationship is used to infer the instantaneous concentrations of the two species,

$$\tau_\nu = \left(\frac{I}{I_0}\right)_\nu = \exp\frac{-k_{\text{eff}}\, nL}{n_0}.$$

Here, τ_ν is the ratio of the transmitted to the incident intensity of radiation at wavelength ν, n is the number density of the absorbing species (averaged over the line of sight), n_0 is the Loschmidt number $= 2.687 \times 10^{19}$ cm^{-3} at standard conditions, L is the absorption path length, and k_{eff} is the effective absorption coefficient. An effective absorption coefficient is required owing to the finite spectral bandwidth of the optics. Values of k_{eff} were determined for O_3 and NO_2 by calibration.

Fused-silica, step-index macro-optical fibres bring radiation into and out of the test section and limit the spatial resolution of the absorption measurement. The transmitting fibre has a core diameter of 0.6 mm, while the receiving fibre is 1.0 mm in diameter. Hot-wire-anemometer measurements indicate low levels of fibre-optic-probe perturbations (less than 3%) on the mean and fluctuating velocity fields.

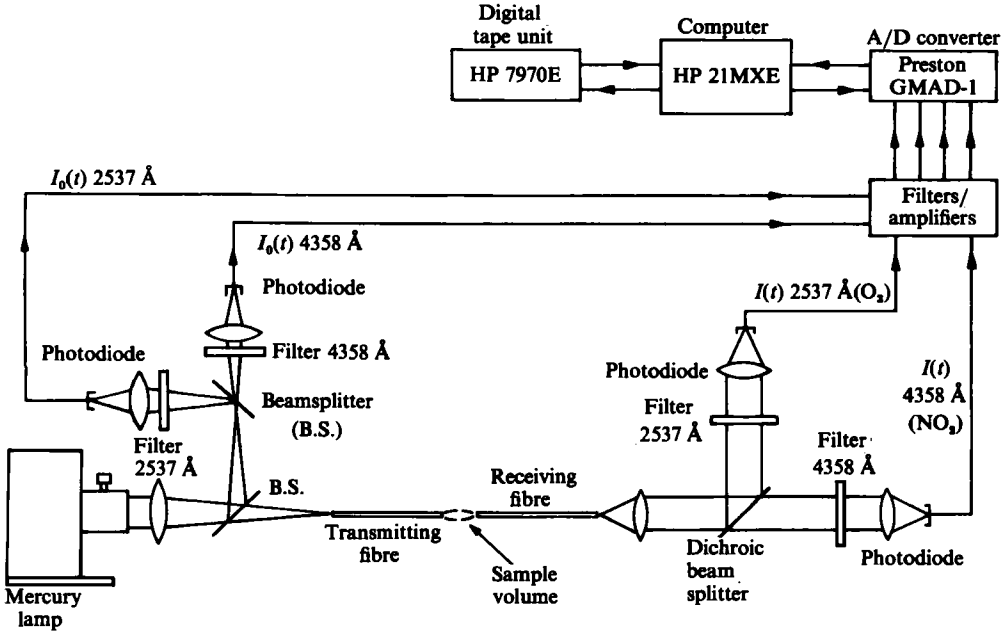

FIGURE 2. Schematic diagram of the fibre-optic probe system.

The spacing between the fibres (absorption path length) can be varied to optimize the signal-to-noise ratio and spatial resolution of the measurements. In the present experiments, two fibre spacings were employed, 10 mm or 5 mm, to obtain information on the effect of probe resolution on the data.

The absorption path was aligned with the spanwise (y) coordinate. For the pre-mixing transition flows investigated, a reasonable degree of spatial uniformity should exist in this direction. With this orientation, the spatial resolution of the measurements in the x- and z-direction varies linearly along the line of sight, between the diameters of the transmitting and receiving fibres, in this case, between 0.6 and 1.0 mm.

At each probe location the O_3 and NO_2 absorption signals were sampled digitally, first at 12.5 kHz and again at 2 kHz in order to resolve the low-frequency portion of the power spectra of the concentration fluctuations. Ten blocks of data, consisting of 1024 points each, were recorded for both species at each sampling rate. These time histories were used to generate the concentration statistics.

In order to visualize the concentration structure of the mixing layer, planar laser-induced fluorescence (PLIF) of NO in a non-reacting flow was employed to obtain instantaneous, two-dimensional maps of the relative concentration of a conserved scalar in the (x, z)-plane, figure 3. The technique used in this experiment has been described in detail by Kychakoff, Howe & Hanson (1984). Briefly, a pulsed beam of light from a Nd:Yag-pumped tunable dye laser is tuned to a resonant frequency of NO, in this case at a wavelength of 225.598 nm, and expanded into a sheet of light by means of a cylindrical lens. This laser sheet passes through fused-silica windows in the top and bottom test-section walls. The resultant NO fluorescence, which is proportional to the NO concentration, is monitored at right angles to the sheet with an image-intensified 100 x 100 element photodiode array. Digital data acquisition and reduction of these fluorescence intensity signals are performed using

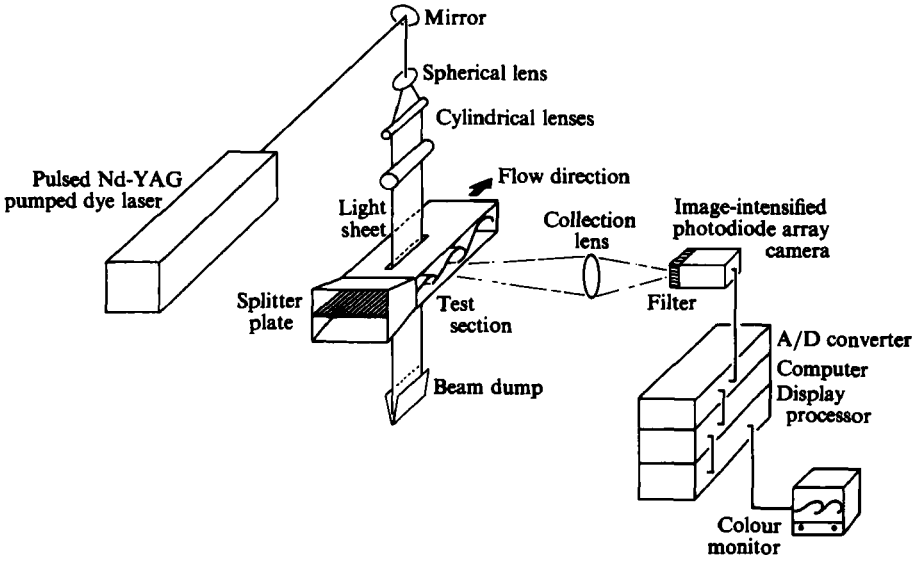

FIGURE 3. Schematic diagram of the planar laser-induced fluorescence (PLIF) optical system.

a buffered camera-to-computer interface and a dedicated computer. Reduced data are displayed on a colour monitor.

The temporal resolution of these measurements is set by the duration of the laser pulse, approximately 8 ns. Since this time is much shorter than any of the physical times associated with the flow, the data represent an instantaneous picture of the planar NO concentration field. With the present configuration of the collection optics, each element in the photodiode array sees a region in the sheet of dimensions 0.33 mm × 0.33 mm, which is the spatial resolution of the data in the x- and z-directions. The thickness of the laser sheet, approximately 0.2 mm in these experiments, determines the spatial resolution in the y-direction.

Streamwise velocity data were obtained in non-reacting (N_2 only) flows using a single-wire, gold-plated hot-wire probe (1.25 mm active sensor length; 5 μm diameter) and a TSI anemometer and linearizer. A programmable digital integrating voltmeter was employed to obtain time-averaged values of velocity. Integration times of 5–10 s were typical. Local r.m.s. velocity fluctuations were determined by coupling the linearizer output to a true r.m.s. voltmeter. Frequency spectra of these velocity fluctuations were generated using a Brüel and Kjaer heterodyne analyser. The velocity data obtained in the non-reacting flow are expected to be valid for the corresponding reacting-flow cases, owing to the very low energy release in these experiments ($\Delta T < 7$ K).

4. Experimental results: non-reacting mixing layer

Experiments were performed in a non-reacting mixing layer to establish the hydrodynamic characteristics and the entrainment and mixing properties of the flow in the regime prior to the onset of the mixing transition. The statistics of the streamwise velocity and the conserved-scalar fields were obtained from temporally and spatially resolved measurements of these variables. In these experiments, the ratio of free-stream mean velocities, $r = \overline{U}_\ell/\overline{U}_h$, was fixed at 0.5, with $\overline{U}_\ell = 3.0$ m/s

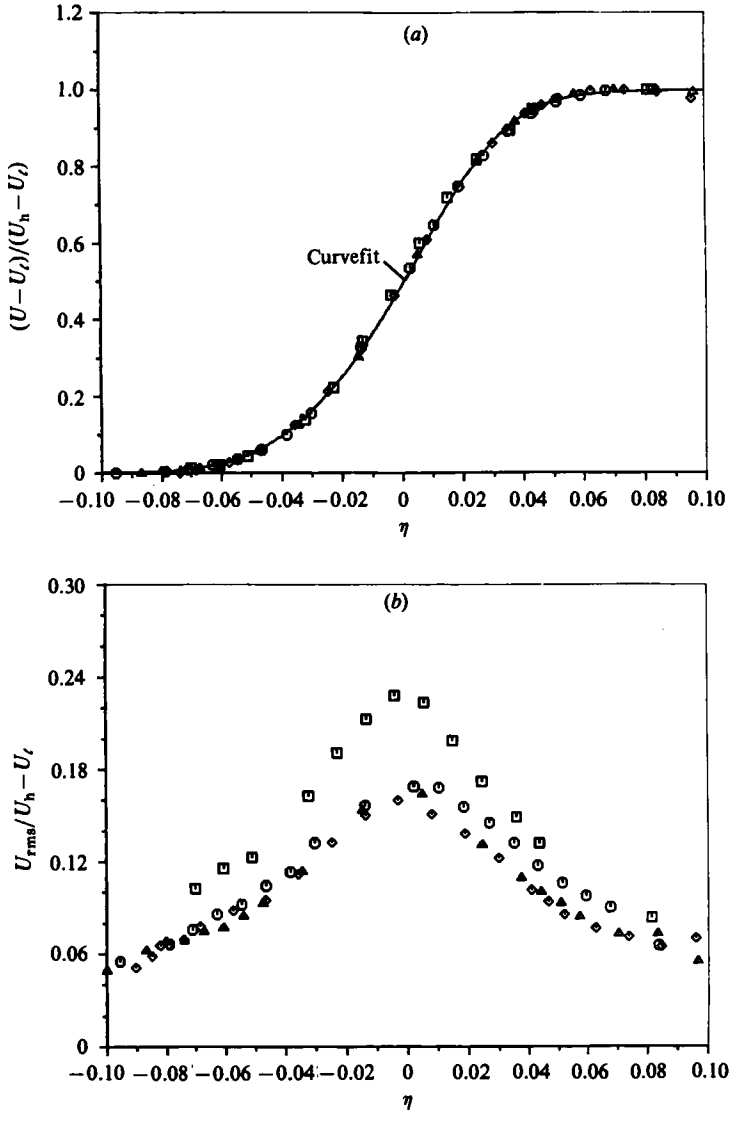

FIGURE 4. Normalized streamwise velocity profiles. The virtual origin of the mixing layer is $x_0 = -0.28$ cm: (*a*) mean velocity; (*b*) r.m.s. velocity. ▣, $x = 5$ cm; ⊙, 12 cm; △, 15 cm; ◇, 18 cm.

and $\overline{U}_h = 6.0$ m/s. The subscripts ℓ and h denote conditions in the low-speed and high-speed streams respectively. The mean velocity ratio was chosen to fall within the range of values of previous studies, while the specific values of $\overline{U}_\ell$ and $\overline{U}_h$ were selected so that pre-mixing transition conditions would prevail throughout most of the flow (Konrad 1976; Breidenthal 1981; Koochesfahani 1984).

4.1. *Velocity measurements*

Velocity measurements in the mixing layer formed from two streams composed of pure N_2 were obtained at five different streamwise locations, corresponding to $x = 0$ (the trailing edge of the splitter plate), 5.0, 12.0, 15.0 and 18.0 cm.

For the free-stream velocities used, the inlet mean velocity profiles within the core

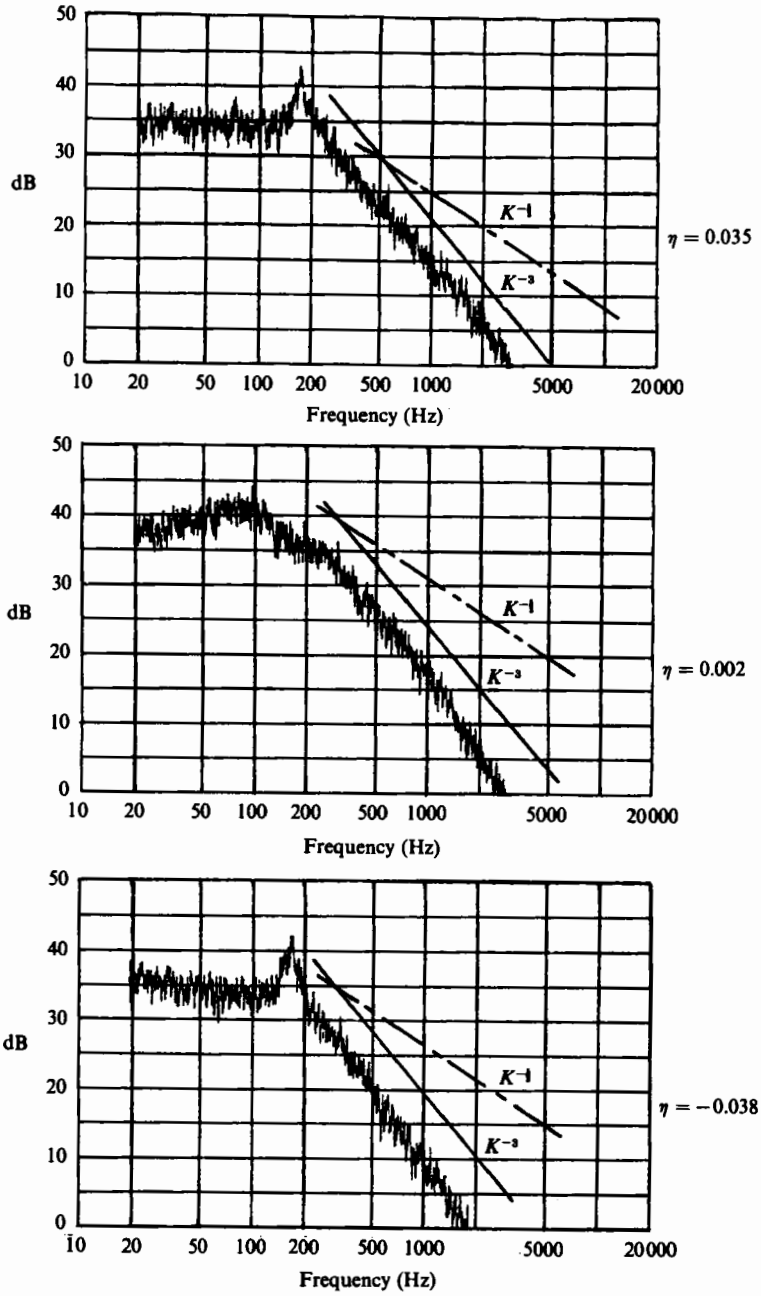

FIGURE 5. Velocity power spectra at three transverse locations in the mixing layer. The straight lines represent power-law decay $\approx K^n$, for $n = -\frac{5}{3}$ and -3.

flow were uniform to within $\pm 0.7\%$, with streamwise turbulence intensities, $u_{\rm rms}/\overline{U} < 0.5\%$. The splitter-plate boundry layers of both streams were laminar in form at separation, with a momentum thickness on the high-speed side of 0.24 mm, and 0.28 mm on the low-speed side.

In figure 4, the normalized mean and r.m.s. velocities are plotted against the similarity variable, $\eta = (z-z_0)/(x-x_0)$, for streamwise locations between $x = 5.0$ and

18.0 cm. The velocity data span a range of $Re_\delta = 730$ and 2520 and $x/\theta_i = 205$ and 738, where Re_δ is the Reynolds number based on $\Delta U = \overline{U}_h - \overline{U}_\ell$ and the vorticity thickness and θ_i is the high-speed splitter-plate boundary-layer momentum thickness. These data indicate that the normalized mean velocity profiles relax to an equilibrium distribution similarity by $x = 5.0$ cm ($x/\theta_i = 205$), while the normalized r.m.s. velocity does not attain similarity in η until $x > 12.0$ cm ($x/\theta_i > 500$). The mean-velocity data can be used to establish the rate of growth of the layer vorticity thickness, $d\delta_\omega/dx = 0.0706$. This growth rate is 15–20% larger than the values calculated from the correlations suggested by Brown & Roshko (1974) and Browand & Latigo (1979), but is within the scatter of existing data.

Three examples of the power spectra of the velocity fluctuations in the mixing layer are shown in figure 5. These spectra were obtained at $x = 12.0$ cm at different z-positions, corresponding to locations near the low-speed edge ($\eta = -0.038$), centre ($\eta = 0.002$) and high-speed edge ($\eta = 0.035$) of the layer. At the edges of the mixing region, a prominent spectral peak at approximately 170 Hz is observed. This peak, which is not evident near the centre of the layer, correlates well with a characteristic frequency of the observed concentration fluctuations (see §4.2), and appears to be associated with the passage of large vortical structures over the probe. Another feature of these spectra is the decay rate with increasing frequency. Expressing the frequency in terms of a wavenumber, $K = 2\pi f/\Delta U$, and assuming a power-law decay of the form K^n, the present data appear to follow a decay law with $n = -3$, rather than $-\frac{5}{3}$, for frequencies greater than 200 Hz. Comparison of the spectra with the experiments of Jimenez, Martinez-Val & Rebollo (1979) suggests a strongly two-dimensional turbulence field, characteristic of pre-mixing transition conditions.

4.2. *Concentration measurements*

Measurements of non-reacting (conserved) scalar concentrations in the mixing layer were obtained in experiments in which one stream was seeded with either O_3 or NO, while the other stream consisted of pure N_2.

In the first series of experiments, O_3 was introduced into the low-speed (3 m/s) stream at concentrations of approximately 1000 p.p.m.V. The fibre-optic absorption probe was traversed vertically through the layer at three streamwise locations: $x = 7.00$, 11.05 and 14.85 cm, corresponding to $x/\theta_i = 290$, 450 and 610 and $Re_\delta = 1000$, 1560 and 2090 respectively. The midpoint of the absorption path, in all of the fibre-optic-probe experiments, was fixed at $y = 4.0$ cm.

The concentration data are expressed in terms of the normalized O_3 mole fraction $\xi(x,t)$:

$$\xi(x,t) \equiv \frac{X^{O_3}(x,t)}{X^{O_3}_s} = \frac{\text{local } O_3 \text{ mole fraction}}{O_3 \text{ mole fraction in low-speed stream}}.$$

Since, by definition, $\xi_\ell = 1$ and $\xi_h = 0$, the normalized O_3 mole fraction is identical with the mixture fraction in a reacting flow with the same hydrodynamic properties as the non-reacting mixing layer (Masutani 1985).

In figure 6(*a*), $\overline{\xi}$ is plotted as a function of the similarity variable $\eta' = (z - z_0')/(x - x_0')$, where x_0' and z_0' are the concentration analogues of x_0 and z_0. Within the uncertainty of the experiments (estimated to be ± 0.03 in ξ), the $\overline{\xi}$ profiles appear to have achieved similarity when plotted against η'. However, there is some evidence that, in the region between $\eta' = 0.03$ and 0.09, the $\overline{\xi}$-distribution evolves slightly in the downstream direction. The solid curve through the data is a nonlinear least-squares hyperbolic tangent fit of the data similar to that suggested by Mungal (1983). Also shown in figure 6(*a*) is a fit to the normalized mean velocity data. The

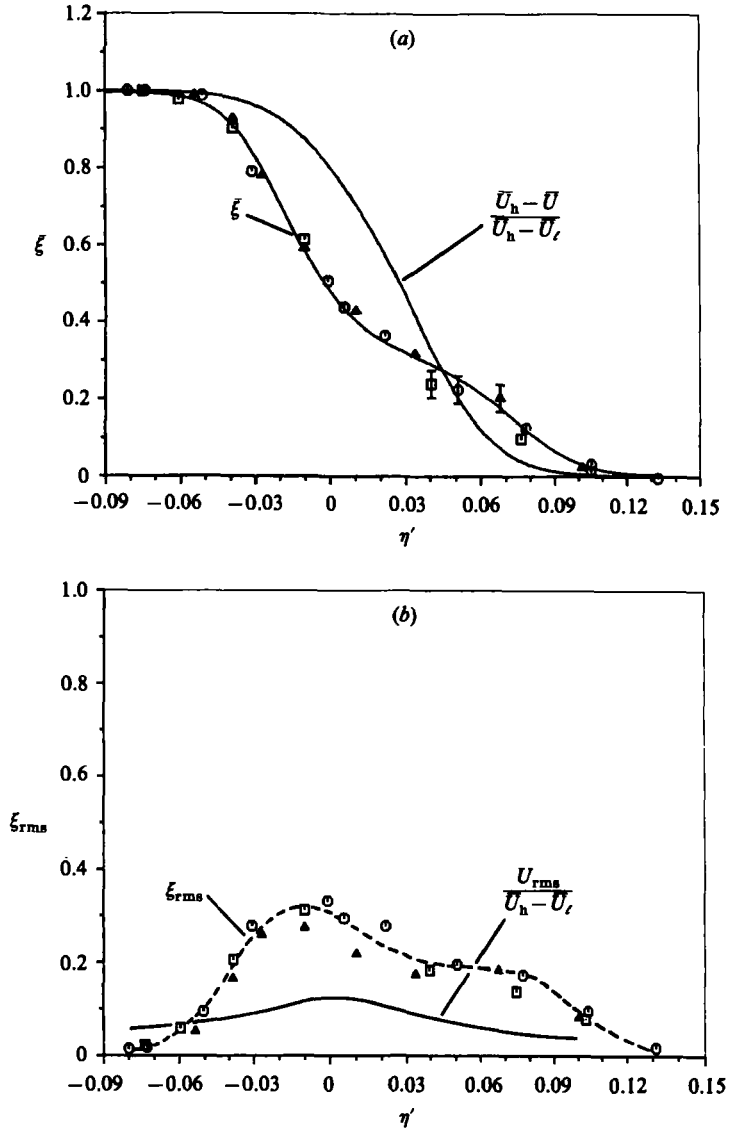

FIGURE 6. Normalized ozone (mixture-fraction) profiles: (*a*) mean profile; (*b*) r.m.s. profile. Included for comparison are curvefits to the velocity data, figure 4. ▣, $x = 7$ cm; ⊙, 11 cm; ▲, 15 cm.

scalar mixing region extends further into the feed streams than does the momentum mixing region, indicating enhanced transport of scalars over momentum, an observation consistent with results of previous mixing-layer studies (e.g. Konrad 1976; Batt 1977).

In figure 6(*b*), the r.m.s. concentration fluctuation is plotted as a function of η'. The quantity ξ_{rms} is indicative of the degree of homogeneity of the flow as observed by a stationary probe. If at some point in the mixing layer only homogeneous fluid appears, then $\xi_{rms} = 0$. Alternatively, if the two streams were composed of immiscible substances then ξ_{rms} would have a maximum value of 0.5 at those points where $\bar{\xi} = 0.5$. The present data never attain a value of 0.5, corresponding to completely

unmixed fluid, but $\xi_{\rm rms}$ does peak near $\eta' = 0$, where, by definition, $\overline{\xi} = 0.5$. Within the scatter of the data, $\xi_{\rm rms}$ attains a self-preserving distribution by $x = 7.0$ cm, indicating that the second moment of the scalar variables relaxes to a similarity condition more rapidly than the dynamical variables. The 'bimodal' shape which is evident in the scalar data is not detected in the velocity data. Konrad (1976) and Batt (1977) have reported similar observations in their studies.

An estimate of the time-averaged fractional volume of fluid originating from the low-speed (O_3-bearing) feed streams V_ℓ that has been entrained into the layer may be obtained from,

$$V_\ell \equiv \frac{1}{|\delta_{\rm h} - \delta_\ell|} \int_{\delta_\ell}^{\delta_{\rm h}} \overline{\xi}(\eta')\, {\rm d}\eta', \tag{4.1}$$

where $\delta_{\rm h}$ and δ_ℓ are the locations of the time-averaged 'boundaries' of the concentration mixing layer; e.g. the points where $\overline{\xi} = 0.01$ and 0.99 respectively. An alternative relation may be derived (Masutani 1985) to calculate the time-averaged fractional flux of low-speed fluid in the layer:

$$\dot{V}_\ell \equiv \frac{\displaystyle\int_{\delta_\ell}^{\delta_{\rm h}} \overline{\xi(\eta')}\,\overline{U(\eta')}\, {\rm d}\eta'}{\displaystyle\int_{\delta_\ell}^{\delta_{\rm h}} \overline{U(\eta')}\, {\rm d}\eta'} + \frac{\displaystyle\int_{\delta_\ell}^{\delta_{\rm h}} \overline{\xi' u'(\eta')}\, {\rm d}\eta'}{\displaystyle\int_{\delta_\ell}^{\delta_{\rm h}} \overline{U(\eta')}\, {\rm d}\eta'}. \tag{4.2}$$

Here, $\dot{V}_\ell$ is the average fraction of the total flow crossing a plane normal to the x-axis that originated from the low-speed stream.

Using the fits to the normalized velocity and concentration data, and ignoring the velocity-scalar fluctuation term in (4.2), integration of (4.1) and (4.2) yields $V_\ell = 0.42$ and $\dot{V}_\ell = 0.34$. These results may be interpreted to mean that approximately 42% of the fluid within the layer originated from the low-speed stream, and that the volume of low-speed fluid passing any streamwise location constitutes 34% of the flow. The corresponding composition ratio

$$E_v \equiv \frac{V_{\rm h}}{V_\ell} = \frac{\text{average volume of high-speed fluid}}{\text{average volume of low-speed fluid}},$$

and entrainment ratio

$$\dot{E}_v \equiv \frac{\dot{V}_{\rm h}}{\dot{V}_\ell} = \frac{\text{average fractional flow rate of high-speed fluid}}{\text{average fractional flow rate of low-speed fluid}},$$

are calculated to be 1.36 and 1.92 respectively. Hence, the rate of entrainment of high-speed fluid exceeds the rate of entrainment of low-speed fluid. Dimotakis (1984) has proposed a simple model, based on geometric arguments, to predict E_v in fully developed mixing layers. For the present free-stream conditions, the Dimotakis model predicts a value of $E_v = 1.23$. This model underestimates slightly the relative rates of entrainment of high-speed fluid into the mixing region. While the present flow cannot be considered to be 'fully developed', the mean velocity and concentration profiles have relaxed to equilibrium distributions in the region of interest, suggesting that the local mean entrainment characteristics of the layer have stabilized by $x = 7.0$ cm.

Examples of time histories of $\xi(t)$, obtained at $x = 11$ cm for several transverse (z) positions, are presented in figure 7. These positions span the width of the mixing layer. In all four traces, a strong regular modulation of the conserved-scalar concentration is observed at a characteristic frequency of 170 Hz.

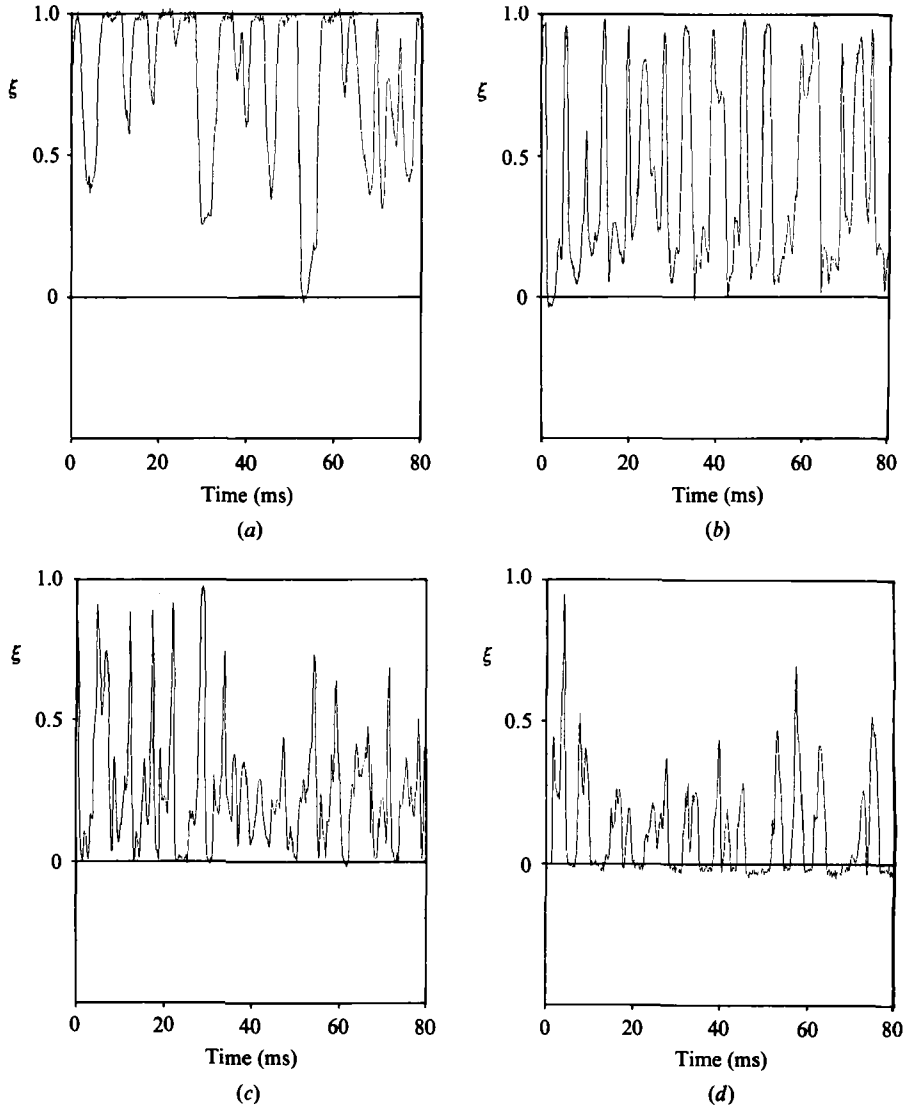

FIGURE 7. Representative mixture-fraction time histories at four transverse locations at $x = 11$ cm: (*a*) $\eta' = -0.031$, (*b*) 0.006, (*c*) 0.051, (*d*) 0.078.

The traces acquired near the low- and high-speed boundaries indicate that, on occasion, free-stream fluid is transported nearly all the way across the mixing region without experiencing dilution. The incursion of unmixed fluid deep within the layer has been observed in many free-shear flows and serves to confirm the importance of the entrainment mechanism of bulk engulfment of free-stream fluid.

The regions of unmixed fluid are bounded by finite-thickness zones composed of fluid that has mixed to some extent. The existence of these zones is indicated by the finite rise and fall times of the strong modulation, figure 8. Since convective velocities of fluid elements through the probe sample volume typically lie between the velocities of the free streams (6 and 3 m/s), a step discontinuity between pure low- and high-speed fluid will result in a transit time across the probe sample volume of

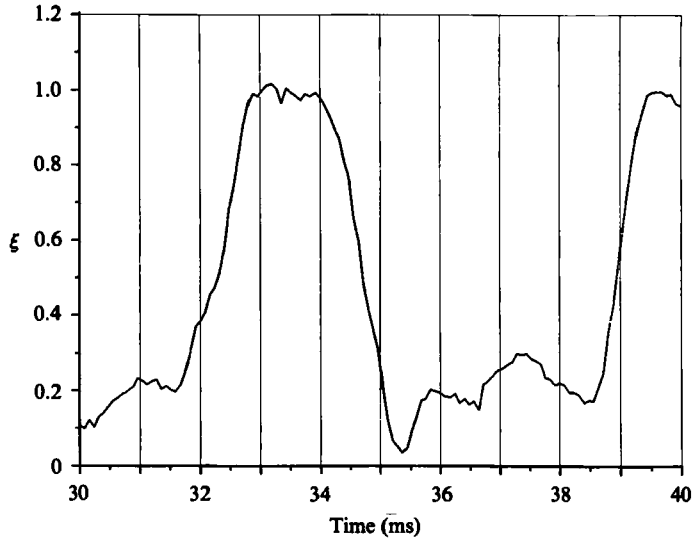

FIGURE 8. Typical rise times of measured normalized O_3 mole fractions at $\eta' = 0.006$ and $x = 11$ cm.

0.3 ms. This transit time is significantly shorter than the 1–3 ms times that are observed. Near the centre of the mixing layer, a lower-amplitude modulation about a 'preferred' value of normalized concentration, $\xi_p \approx 0.2$, occurs, superposed on the large concentration fluctuations.

The time records of ξ may be used to construct probability density functions (p.d.f.s) of the mixture fraction. The p.d.f. is defined in the conventional manner:

$$f(\alpha)\,\mathrm{d}\alpha = \text{probability that } \alpha < \xi < \alpha + \mathrm{d}\alpha,$$

and

$$\int_{-\infty}^{+\infty} f(\xi)\,\mathrm{d}\xi = 1.$$

A representative p.d.f. of the mixture fraction is presented in figure 9 for $x = 11$ cm. Mixture-fraction p.d.f.s at $x = 7$ and 15 cm were qualitatively similar. In these three-dimensional plots, the probability density is given as a function of ξ and the similarity coordinate η'. The plot shows the evolution of the p.d.f. of ξ across the mixing layer.

The spikes in the p.d.f. (i.e. the delta functions broadened by system noise and spatial-averaging effects) at $\xi = 1$ and 0, which persist for some distance into the layer, indicate the presence of pure (unmixed) fluid from either free stream. Instrument noise results in non-zero values of the p.d.f. outside the interval $0 \leqslant \xi \leqslant 1$. Free-stream fluid that has been mixed at the molecular level (or on the level of the resolution of the probe)† accounts for the non-zero values of the p.d.f. in the range $0 < \xi < 1$. The presence of a third peak in the p.d.f. between 0 and 1 indicates that a 'preferred' concentration $\xi_p(x)$ exists for the mixed fluid. The value of $\xi_p(x)$ at a given streamwise location in the flow does not change across the mixing

† The finite spatial resolution of the optical probe results in a measured extent of mixed fluid that is higher than is actually present in the layer. Masutani (1985) has shown that in the present experiments the maximum error in the local fraction of mixed fluid is 0.10.

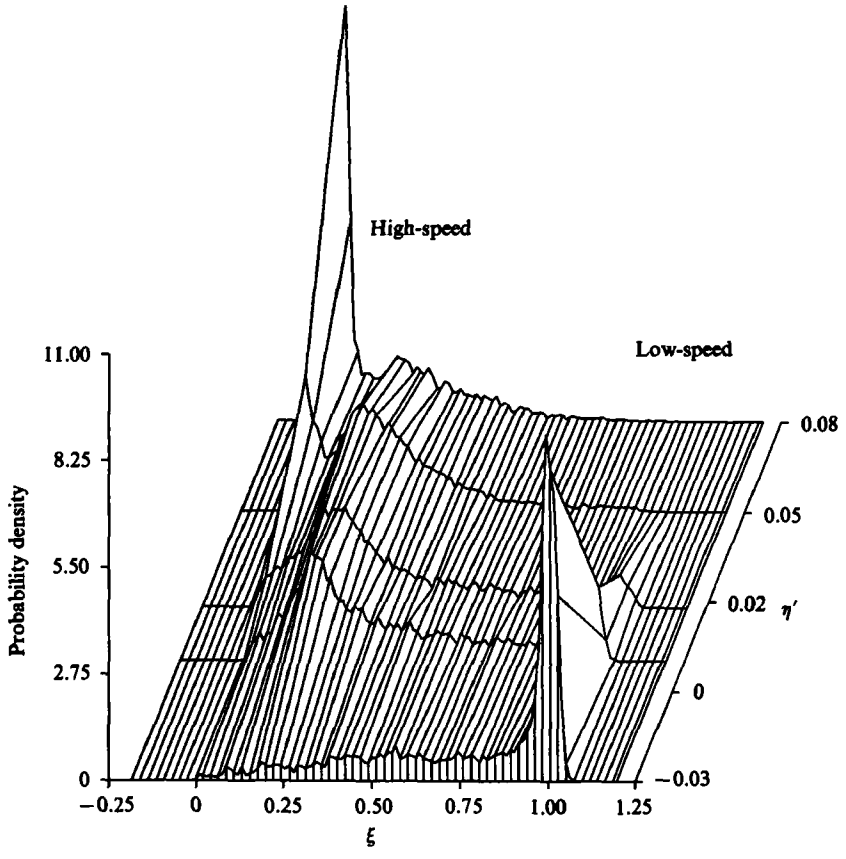

FIGURE 9. Mixture-fraction (conserved-scalar) p.d.f. at $x = 11$ cm. O_3 is in the low-speed stream.

layer, although the height of the peak does vary. Comparison of the p.d.f.s at the various streamwise positions shows that the value of the preferred concentration increases with x, figure 10, from a value of approximately 0.14 at $x = 7.00$ cm to approximately 0.27 at $x = 14.85$ cm. These values of the normalized O_3 concentration that has been mixed at the molecular level may be contrasted with the fractional volume of low-speed (O_3-bearing) fluid that has been entrained into the mixing layer, $V_\ell = 0.42$. While ξ_p appears to be approaching this value of V_ℓ for the present conditions, generally less than 60% of the fluid entrained into the mixing layer is mixed at the molecular level.

Koochesfahani (1984) observed similar p.d.f.s of a conserved scalar in a liquid mixing layer. However, neither a preferred concentration for the mixed fluid nor, for that matter, any significant volume of mixed fluid was detected until after the mixing transition. Upstream of this point, the conserved-scalar p.d.f.s (obtained at $Re_\delta \approx 1300$) are characterized by spikes at 1 and 0, with probability densities only slightly greater than zero for $0 < \xi < 1$. This type of p.d.f. indicates a flow consisting of alternating regions of pure free stream fluid bordered by extremely thin interfacial zones.

The asymmetry in molecular mixing, noted above, may be quantified in terms of a mixing efficiency $FM_{\ell,h} \equiv$ fraction of fluid entrained into the layer from either the

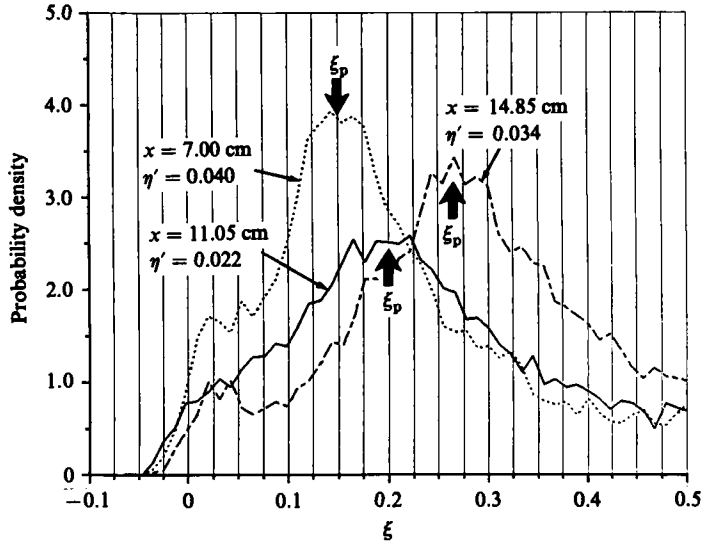

FIGURE 10. Streamwise evolution of the 'preferred' concentration of mixed fluid ξ_p.

low- or high-speed free stream that is mixed at the molecular level. A value of $FM = 0$ indicates that none of the entrained fluid is mixed, while $FM = 1$ implies that the entrained fluid is completely mixed. According to the definition,

$$FM_\ell = \frac{V_\ell - \Delta V_\ell}{V_\ell}, \quad FM_h = \frac{V_h - \Delta V_h}{V_h},$$

where $\Delta V_{\ell,h}$ is the fraction of the unmixed low- or high-speed fluid in the layer,

$$\Delta V_{\ell,h} = \frac{1}{|\delta_h - \delta_\ell|} \int_{\delta_\ell}^{\delta_h} P_{\ell,h}(\eta')\, d\eta',$$

and where $P_{\ell,h}(\eta')$ is the probability of finding unmixed fluid from the low- or high-speed free streams, as determined from the unmixed fluid peaks of the mixture-fraction p.d.f.s. For the conditions of the present experiment, $FM_\ell \approx 0.4$ and $FM_h \approx 0.6$, indicating that the layer is slightly more efficient in mixing fluid entrained from the high-speed free stream.

A global description of the composition of the mixed fluid is given by the mixed-fluid ratio $RM \equiv$ volume of mixed high-speed fluid divided by volume of mixed low-speed fluid. According to this definition,

$$RM = \frac{FM_h}{FM_\ell} E_v.$$

For the present conditions, $RM \approx 2$, indicating that mixed fluid in the layer comprises approximately two parts of fluid from the 6 m/s feed stream and one part from the 3 m/s feed stream.

The structure of the non-reacting, pre-mixing transition gas-phase mixing layer, was visualized in an experiment in which NO was introduced into the high-speed stream at concentrations of approximately 10000 p.p.m.V. The planar laser-induced fluorescence technique (PLIF) was used to obtain instantaneous two-dimensional maps of the NO concentration field. An example of these maps is shown in figure 11 (Plate 1). In this figure flow proceeds from right to left, with the high-speed stream

on top. The map encompasses a region in the flow field lying between the fibre-optic measurement stations at $x = 7$ and 11 cm. The locations of the 0.1 and 0.9 limits of X_{NO}/X_{NO_h}, determined from gas-sampling-probe measurements, are shown for the purpose of orientation. An estimate of the locations of the instantaneous concentration isopleths is presented above the map.

The important features of this figure are the evidence of large-scale concentration structures and finite-thickness diffusion zones, with dimensions on the order of several mm. There is a continuous, distorted interface between the regions of unmixed fluid, with no evidence of discrete packets of free-stream fluid being carried across the layer. As anticipated from the fibre-optic-probe data, there is evidence of nearly homogeneous 'cores' consisting of normalized NO number densities lying between 0.7 and 0.8 (corresponding to $\xi = 0.3$ and 0.2 respectively). Assuming an eddy convective velocity equal to the mean of the free-stream velocities, the frequency associated with the large concentration structures is estimated to be approximately 170 Hz. This frequency correlates with the large-amplitude modulation of O_3 concentration and also corresponds to the peak in the velocity power spectra.

Concentration structures constructed from linear array measurements of fluorescence intensities in a pre-mixing transition liquid layer (Koochesfahani 1984) exhibit marked differences from the present results. In the liquid layer, the interfacial zones are extremely thin and the mixing region appears to be composed almost entirely of unmixed fluid drawn in from the two feed streams. The absence of mixed fluid in the liquid layer is not unexpected given the large differences in the molecular diffusion coefficients of the scalar tracers in water and in gaseous N_2. The observed differences in concentration structure of gas-phase and liquid mixing layers at comparable values of Re_δ indicate the important role of molecular diffusion in the mixing process occurring in the pre-mixing transition flow regime.

To explore further the observed asymmetry in volumetric entrainment rates into the mixing layer from the two feed streams, and the even more pronounced asymmetry in molecular mixing, the velocity of the O_3-bearing feed stream was increased to 6 m/s, while the pure N_2 feed-stream velocity was reduced to 3 m/s; hence, the hydrodynamic field was not changed. In this 'flip' experiment, data were obtained with the fibre-optic probe at $x = 7$ and 11 cm, with a maximum free-stream O_3 concentration of approximately 560 p.p.m.V (due to limitations of the ozonator). Similar experiments have been performed previously in a liquid mixing layer (Koochesfahani & Dimotakis 1984) and in an H_2–F_2 reacting mixing layer (Mungal 1983).

A 'flip' mixture fraction, $\xi^f(x,t)$ may be defined as

$$\xi^f(x,t) \equiv \frac{X^{O_3}(x,t)}{\overline{X_h^{O_3}}} = \frac{\text{local } O_3 \text{ mole fraction}}{O_3 \text{ mole fraction in high-speed stream}}.$$

The p.d.f. of ξ^f, obtained at $x = 11.0$ cm, is presented in figure 12. Since from symmetry considerations

$$\xi^f(x,t) = 1 - \xi(x,t),$$

it follows that the p.d.f. of ξ^f should be a reflection of the corresponding p.d.f. of ξ about $\bar{\xi} = 0.5$. This implies that ξ_p^f ($x = 11$ cm) should be located at $1 - \xi_p$ ($x = 11$ cm) ≈ 0.79, which is what is observed. Moreover, as observed in the non-flip experiment, ξ_p^f does not vary across the layer, but does shift to lower values of ξ^f with increasing distance from the splitter plate, indicating increasing proportions of low-speed fluid in the homogeneous zones.

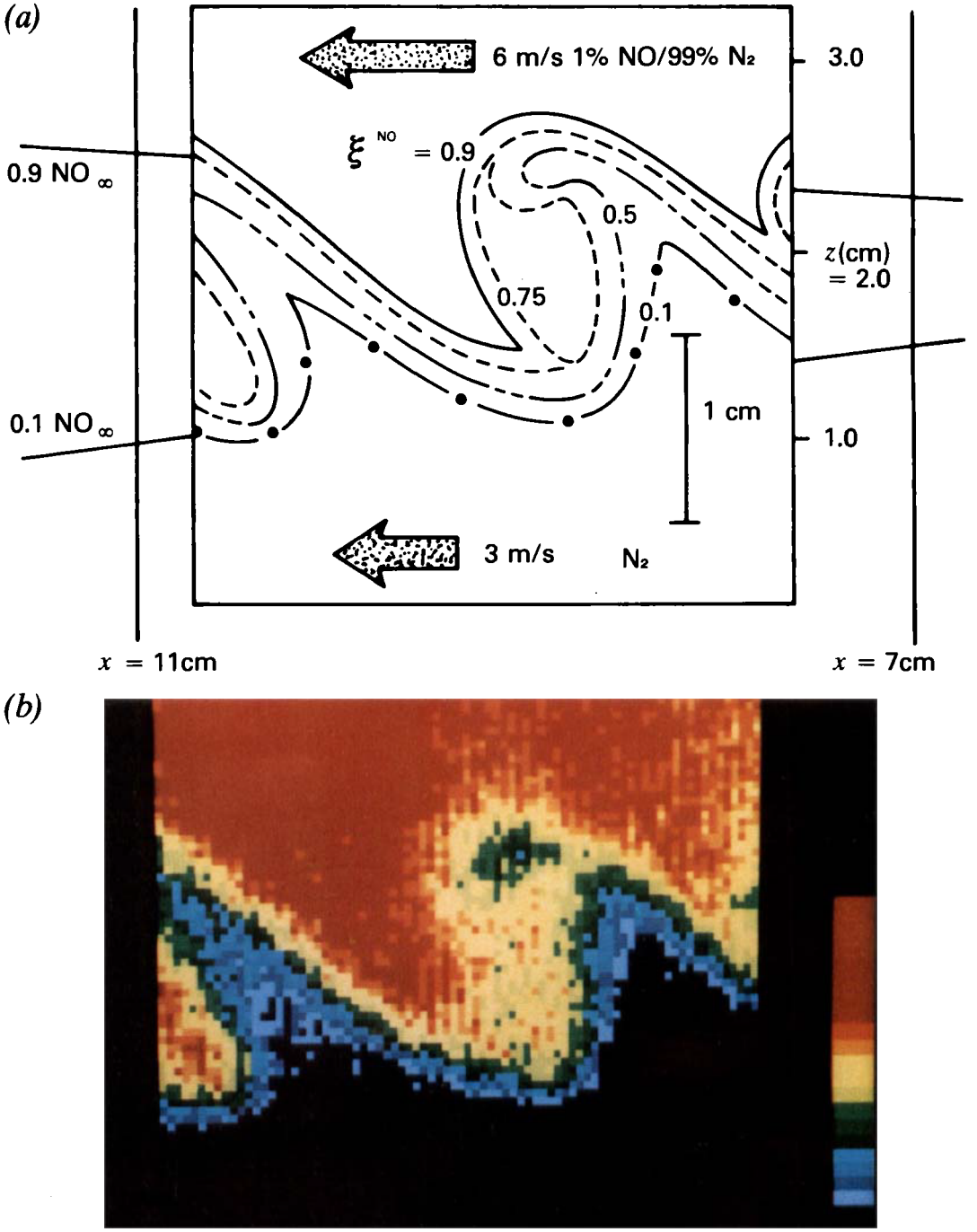

FIGURE 11. NO concentration (conserved-scalar) isopleths: *(a)* instantaneous NO concentration map; *(b)* planar laser-induced fluorescence (PLIF) flow image.

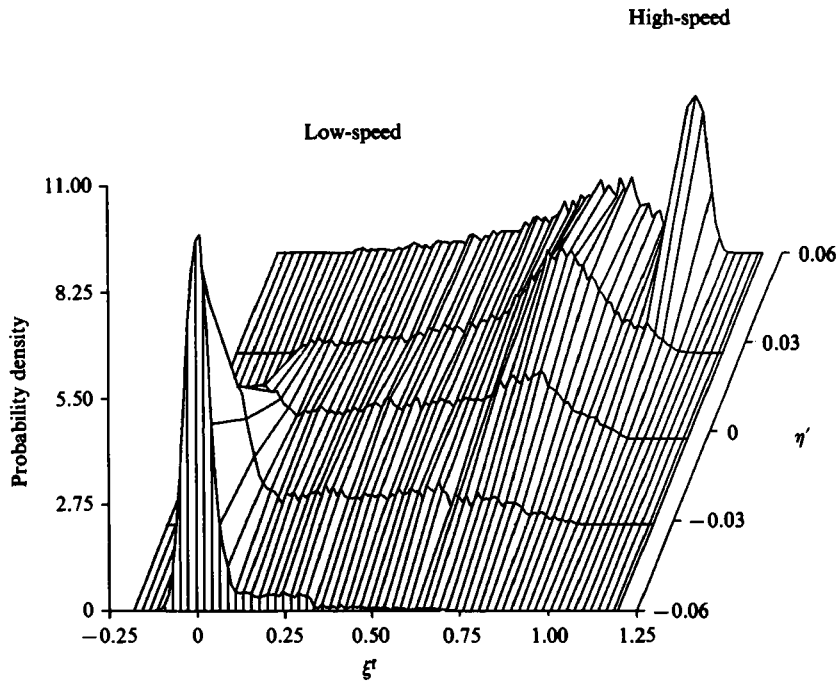

FIGURE 12. Mixture-fraction p.d.f. at $x = 11$ cm for the non-reacting 'flip' experiment. O_3 is in the high-speed stream.

The mixing efficiencies FM determined from the p.d.f.s in the flip experiments and the mixed-fluid ratio RM are identical with those observed in the non-flip experiments, indicating that the entrainment and mixing processes are the same in these two situations.

The results of these flip experiments confirm the observations of previous mixing-layer studies (Mungal 1983; Koochesfahani & Dimotakis 1984) that, on average, entrainment favours an excess of high-speed fluid. In addition, the flip experiments confirm the observation that the layer is more efficient in mixing fluid entrained from the high-speed free stream.

5. Observations on structure, entrainment and mixing of the non-reacting mixing layer

The experimental data discussed above suggest that prior to the mixing transition, the fluid in the plane mixing layer exists in three states: tongues of unmixed free-stream fluid which, on occasion, stretch all the way across the layer; finite-thickness interfacial diffusion zones of mixed fluid which border the volumes of unmixed fluid; and cores of mixed fluid of nearly homogeneous composition, corresponding to ξ_p. The interfacial diffusion zone separating unmixed fluid is a continuous distorted interface, with no evidence of discrete packets of free-stream fluid being carried across the layer. This structure is consistent with that postulated by Broadwell & Breidenthal (1982). In addition, the velocity and concentration spectra exhibit a distinct K^{-3} decay with frequency, indicative of a flow field dominated by two-dimensional effects. These spectra also show a strong 170 Hz modulation associated with the large-scale longitudinal vortical structures. The data

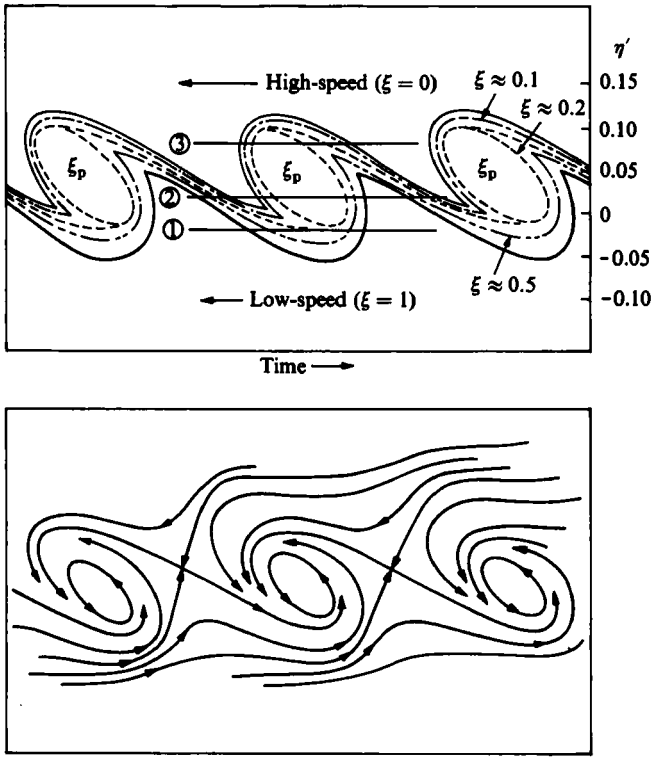

FIGURE 13. Inferred concentration structure and flow patterns of the pre-mixing transition mixing layer.

obtained in the present study, when combined with flow-visualization results from previous plane-mixing-layer studies, suggest an instantaneous concentration-field structure of the type shown in figure 13. Also included in this figure is a sketch of the assumed streamlines in the frame of reference of the primary vortical structures. This flow pattern is suggested by the calculations of Corcos & Sherman (1976), and has been proposed by Coles (1981). Similar flow patterns have been employed by Konrad (1976) and Broadwell & Breidenthal (1982).

In figure 14, representative concentration time histories of $\xi(t)$, obtained with the fibre-optic probe at three locations in the mixing layer, are compared with the concentration time histories inferred by translating a probe through the hypothetical structures depicted in figure 13. These inferred time histories are assumed to be recorded by a concentration probe moving at constant velocity, from left to right, along the horizontal lines marked 1, 2 and 3. The normalized timescale t/τ, where τ is the passage time of the large structures, is expanded in the upper figure for clarity. The strong qualitative similarities between the actual and hypothetical time histories support the proposed structure.

The concentration structure and flow patterns depicted in figure 13 suggest that entrainment and mixing of free-stream fluid proceed by a process of engulfment, diffusional mixing and ingestion into the homogeneous core flow regions. In this process, free-stream fluid penetrates deep within the mixing region, drawn in by the velocity field induced by the primary vortices. These volumes of gas from the two feed streams are brought into contact and interfacial diffusional mixing zones form. These regions are characterized by large continuous spatial gradients of concentration.

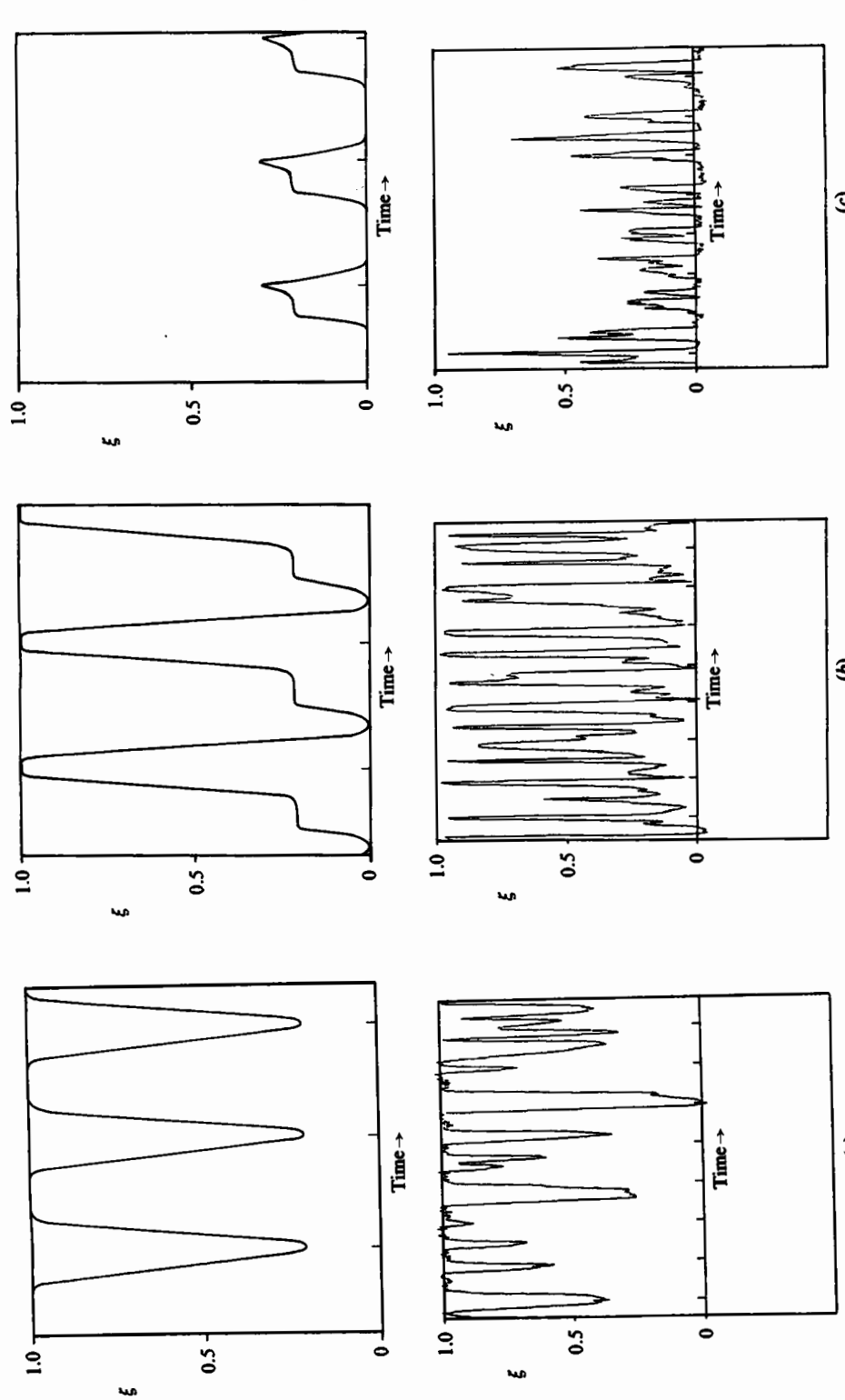

FIGURE 14. Comparison of measured mixture-fraction time histories (lower) and the time histories associated with the inferred concentration structure of figure 13(*a*). The experimental traces are those plotted in figure 7(*a*, *b*, *d*). The timescales in the two plots are normalized by τ, the passing time of the large-scale structures.

The continuous gradients imply that molecular diffusion, perhaps accelerated by the induced strain fields, is a major mechanism for mixing in these interfacial regions. Eventually, this mixed fluid is incorporated into the cores.

Free-stream fluid may bypass the diffusional mixing process and be drawn directly into the core regions during vortex pairing events. Flow-visualization images of pairing (e.g. Winant & Browand 1974; Roshko 1976; Koochesfahani 1984) indicate that this process consists of a vortex overtaking and climbing over an adjacent vortex, in the course of which the intervening interfacial diffusion zone, as well as a quantity of free-stream fluid, is trapped within the new core.

The manner in which fluid from the free streams is ingested into the core regions determines whether these regions will be active centres of reaction in a chemically reacting flow. If chemical-reaction times are short relative to the contact time of free-stream reactants in the interfacial zones, then fluid that is incorporated into the core regions will comprise product species, residual rich reactants and diluent gas. In this situation the homogeneous regions will be repositories for 'old' fluid, and reaction will be confined to the interfacial layer. However, if reaction rates in the interfacial layers are slow or if fresh reactants are ingested directly in the core regions, then these regions will become active centres of reaction.

The mixture-fraction p.d.f.s indicate a slow evolution of the concentration structure of the mixing layer, as evidenced by the increase in the preferred concentration of mixed fluid ξ_p. This increase can occur only by an increase in the proportion of the low-speed fluid in these core regions since there is no evidence that the composition or fractional volume of fluid in the interfacial diffusion regions increases with x (Masutani 1985). The experimental trends suggest the persistence of a large initial bias toward the entrainment of high-speed fluid. Koochesfahani & Dimotakis (1984) have suggested that, during the first roll-up of the longitudinal vortex structure, a significant excess of high-speed fluid is incorporated into the vortex core region. Subsequent to this event, the entrainment and mixing rates stabilize, and increased volumes of low-speed fluid are drawn into the core, or are ingested during pairing events. The nearly uniform concentration structure in these zones continues to evolve as the large vortical structures are convected downstream, ultimately attaining a concentration determined by the average relative entrainment rates of fluid from the two free streams into the core. A semi-empirical model based on the type of dilution process described above (Masutani 1985) qualitatively describes the spatial evolution of ξ_p.

6. Experimental results: reacting mixing layer

In these experiments, one feed stream contained O_3 in N_2 carrier gas, while the other contained varying amounts of NO in N_2. Fibre-optic-probe measurements were conducted for three different values of overall lean-to-rich reactant ratio ϕ:

$$\phi \equiv (X_{O_3})_\infty/(X_{NO})_\infty,$$

where X_∞ represents the feed-stream mole fraction of the reactant. In three experiments, O_3 was in the low-speed stream and NO, in excess of stoichiometric proportions, was in the high-speed stream. In these tests, the NO concentration was varied over an order of magnitude, while the O_3 concentration was held fixed at approximately 1000 p.p.m.V. In order to determine the effect of probe spatial resolution on the concentration measurements, two different fibre spacings (10 and 5 mm) were employed in a number of these experiments. A flip experiment (with O_3

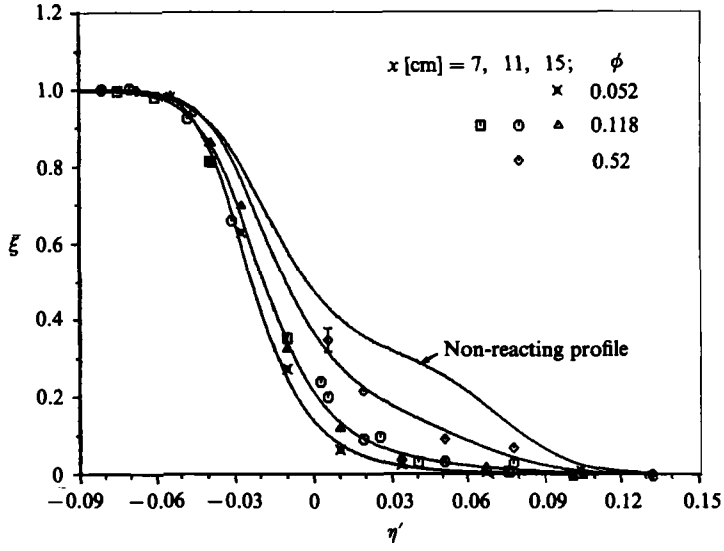

FIGURE 15. Normalized mean O_3 mole fraction in reacting flows for three reactant ratios. Also shown is a fit to the non-reacting flow results.

in the high-speed stream and NO in the low-speed stream) was conducted for a value of ϕ equal to one of the values employed in the non-flip experiments, in order to assess the effect of asymmetric entrainment and mixing on the structure of the reacting mixing layer.

6.1. *Reactant* (O_3) *concentration measurements*

In figure 15, mean values of the normalized reactant (O_3) concentration $\bar{\xi}_R$ are plotted as a function of η' for the three values of ϕ used in the non-flip experiments. Also included in the figure is a fit to the non-reacting O_3 profile shown in figure 6 (*a*). As anticipated, chemical reaction depletes the mean O_3 concentration in the layer. For a fixed value of ϕ, the data indicate that the $\bar{\xi}_R$ profiles appear to attain similarity for $x > 7.0$ cm. Although NO was in significant excess of stoichiometric proportions for all of the experiments, increasing the NO concentration, while holding the O_3 concentration fixed, results in reduction of the lean-reactant (O_3) concentrations in the layer.

Reactant species must be mixed at the molecular level for reaction to occur. Free-stream fluid that has been entrained into the mixing layer, but remains unmixed (corresponding to $\xi_R = 1$), will not undergo reaction. A comparison of the p.d.f.s of the reactive scalar ξ_R with those of the passive scalar ξ at the same locations should show significantly reduced probability densities for $0 < \xi < 1$, corresponding to depletion of the volume of mixed reactant (O_3) in the reacting layer, with the 'spikes' at ξ, $\xi_R = 1$ remaining unchanged. A reactive-scalar p.d.f. is shown in figure 16. Comparison of figures 9 and 16 shows that chemical reaction produces the expected reduction in the probability densities of mixed fluid. However, it appears that, contrary to expectations, the height of the spike in the p.d.f. at $\xi_p = 1$ also has been reduced by chemical reaction. This reduction in the probability P_ℓ of finding unmixed O_3-bearing free-stream fluid in the reacting flow is quantified in figure 17. These data indicate that chemical reaction reduces the probability of finding unmixed lean reactant throughout the mixing layer, and that the extent of depletion of unmixed fluid increases as the free-stream NO concentration increases.

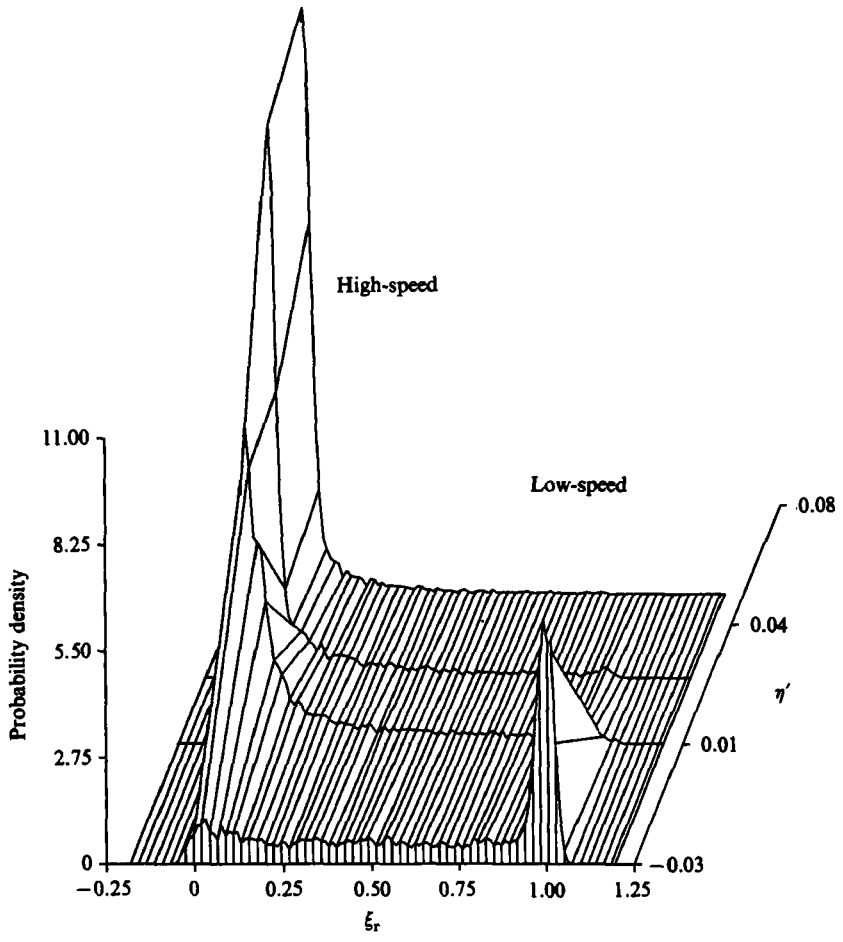

FIGURE 16. Reactive scalar p.d.f. for a reacting flow at $x = 11$ cm, $\phi = 0.118$. O_3 is in the low-speed stream; NO is in the high-speed stream.

Additional insight into the structure of the reacting mixing layer is gained by comparing the mixed-fluid probability P_m for three reacting flows with the non-reacting flow, figure 18. The quantity P_m is defined as

$$P_m \equiv \int_{0+\delta_0}^{1-\delta_1} f(\xi, x)\, d\xi, \tag{6.1}$$

where δ_0 and δ_1 are chosen to exclude contributions of system noise to P_m near $\xi = 0$ and 1. In (6.1), P_m is the fraction of fluid at a point in the mixing layer that has been mixed at least at the level of the probe resolution. As expected, in the reacting flows the probability of finding O_3 in concentrations other than $\xi = 0$ or 1 is lower than in the non-reacting layer, and the probability decreases as the free-stream NO concentration increases.

The data in figures 15 and 18 indicate that, by increasing the free-stream concentration of the rich-reactant species (NO), a larger fraction of the lean reactant (O_3) that has been entrained into the layer is consumed by chemical reaction. However, in the present experiments, a significant fraction of the mixed lean reactant remains unreacted.

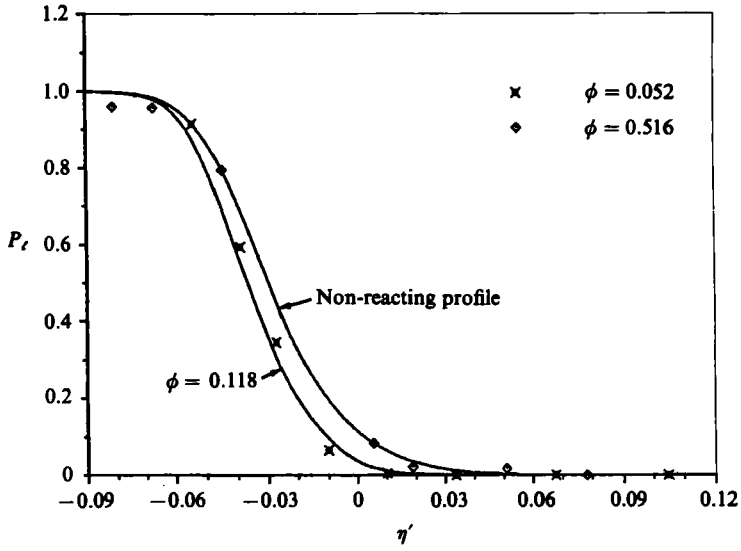

FIGURE 17. Probability of finding unmixed O_3-bearing free-stream fluid in the mixing layer for non-reacting and reacting flows.

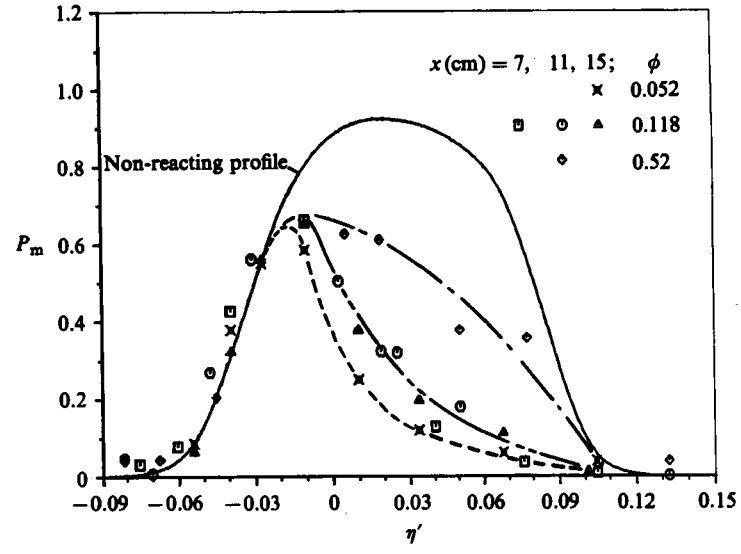

FIGURE 18. Probability of finding mixed O_3-bearing free-stream fluid in the mixing layer (see equation 6.1) for non-reacting and reacting flows.

In experiments performed with variable fibre spacings, there were no discernible differences observed in the $\bar{\xi}_R$ and $(\xi_R)_{rms}$ profiles or in the concentration power spectra as the probe resolution was decreased from 10 mm to 5 mm, suggesting a reasonable degree of spanwise uniformity.

The impact of the asymmetric entrainment and mixing characteristics of the layer on chemical reaction was examined in the flip experiments. A comparison of the mixed-fluid probabilities for the non-flip and flip reacting-flow experiments reveals some striking differences, see figure 19. Exchanging O_3 and NO between the free

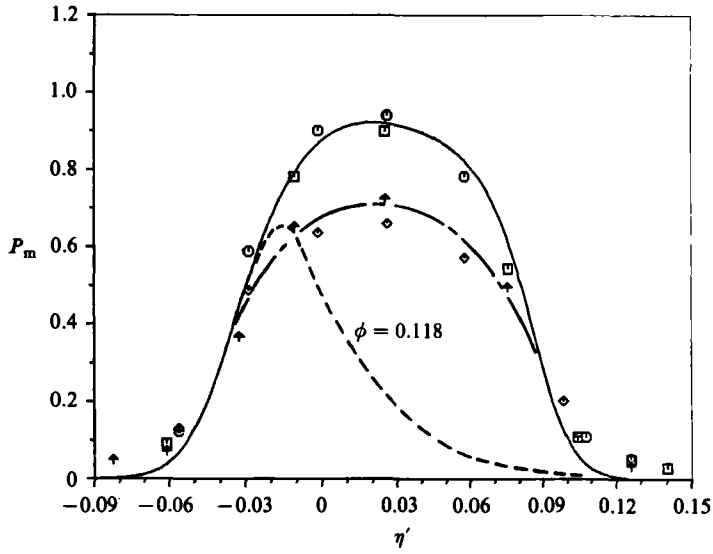

FIGURE 19. Mixed-fluid probability for non-reacting (□, $x = 7$ cm; ○, 11 cm) and reacting (♠, $x = 7$ cm, ◆, 11 cm) flows for the flip experiments, $\phi = 0.110$. The dashed line is the corresponding reacting-flow profile for the non-flip experiment.

streams produces a noticeable change in the volume of the fluid in the layer containing mixed, but unreacted lean-reactant species. While more product forms in the flip configuration, as expected because of the higher mixing efficiency for high-speed fluid, the probability of finding mixed, but unreacted, O_3 is higher. Although the ratio of NO-to-O_3 free-stream concentrations was held nearly constant, the absolute values of the NO and O_3 concentrations were reduced in the flip experiment, owing to the limitations of the ozonator. Hence, characteristic chemical times in the flip experiment were longer, while scalar transport times remained the same. It is likely, then, that slower reaction rates in the flip experiment will result in larger volumes of partially reacted fluid, which will persist and penetrate deeper into the mixing region.

6.2. *Product* (NO_2) *concentration measurements*

The $NO + O_3 \rightarrow NO_2 + O_2$ reaction is irreversible for the present experimental conditions. The product species, once formed, behave as inert scalars, being dispersed by macroscopic and molecular transport processes, and accumulated within the mixing region. Measurements of NO_2 at a fixed location in the flow reflect, therefore, the sum of reaction and mixing events.

The NO_2 concentrations may be normalized by the mean value of the O_3 mole fraction in the free stream,

$$\zeta(x,t) \equiv \frac{X_{NO}(x,t)}{\overline{X_{\infty}^{O_3}}}.$$

Masutani (1985) has shown for isothermal flows that, in addition to direct measurement, $\overline{\zeta}(x)$ can be determined from data on $\overline{\xi}$ and $\overline{\xi}_R$:

$$\overline{\zeta}(x) = \overline{\xi}(x) - \overline{\xi}_R(x). \tag{6.2}$$

Equation (6.2) provides an independent means to obtain the time-averaged normalized product mole fractions, which may be compared with the values measured by

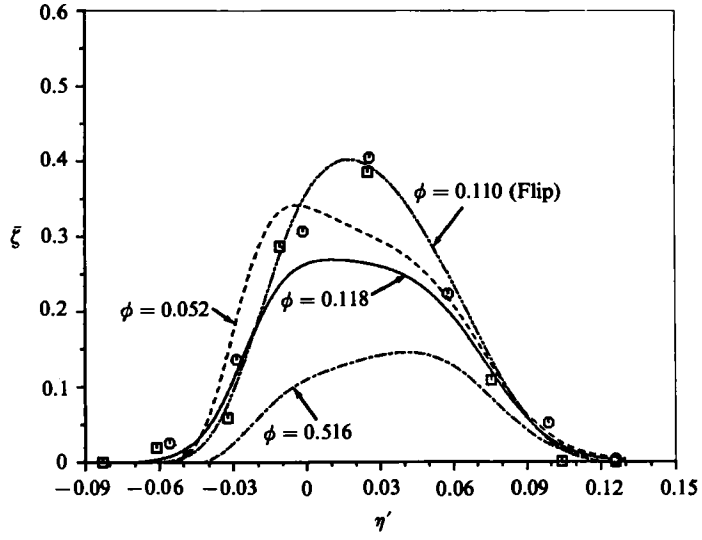

FIGURE 20. Mean normalized product concentration for the non-flip and flip reacting flow experiments. ◻, $x = 7$ cm; ⊙, 11 cm.

the fibre-optic probe. This comparison is useful since the signal-to-noise ratio of the NO_2 measurements was significantly smaller than for the O_3 measurements, owing to differences in absorption coefficient of the two species.

Profiles of $\bar{\zeta}$ are presented in figure 20. In the non-flip experiments changing the free stream concentration of rich reactant NO alters the mean product distribution in the layer. As $(X_{NO})_\infty$ is increased from 2000 to 8500 p.p.m.V ($\phi = 0.516$ and 0.118 respectively), with $(X_{O_3})_\infty$ held fixed, there is a marked increase in both the peak value of $\bar{\zeta}$ and the total (integrated) amount of product in the layer. The increase is less pronounced as the free-stream mole fraction is increased further to 19000 p.p.m.V. For the lower overall reactant ratios, the mean product distribution is skewed toward the low-speed edge of the mixing layer. Mungal (1983) observed that the peak values of mean temperature in a post-mixing transition $H_2 + F_2$ mixing layer were shifted off the layer centreline, toward the free stream bearing the lean reactant.

Switching the lean reactant from the low-speed stream to the high-speed stream results in a significant increase in the magnitude of $\bar{\zeta}$ throughout most of the mixing layer, with a modest skewing of the mean product distribution toward the lean-reactant (high-speed) free stream.

The effects of the asymmetric mixing properties of the layer, as well as the influence of feed-stream reactant concentrations on the amount of product formed in the layer, may be quantified by integration of the experimental profiles of $\bar{\zeta}$,

$$\Pi \equiv \frac{1}{|\delta_h - \delta_\ell| V_{O_3}} \int_{\delta_\ell}^{\delta_h} \bar{\zeta}(\eta')\, d\eta',$$

where V_{O_3} is the fractional volume of fluid in the layer from the free stream containing O_3, equation (4.1). The quantity Π may be interpreted as the fraction of the volume of O_3-bearing fluid, present in the layer under non-reacting-flow conditions, that has undergone chemical reaction. The product thickness P/δ_ω employed by Breidenthal

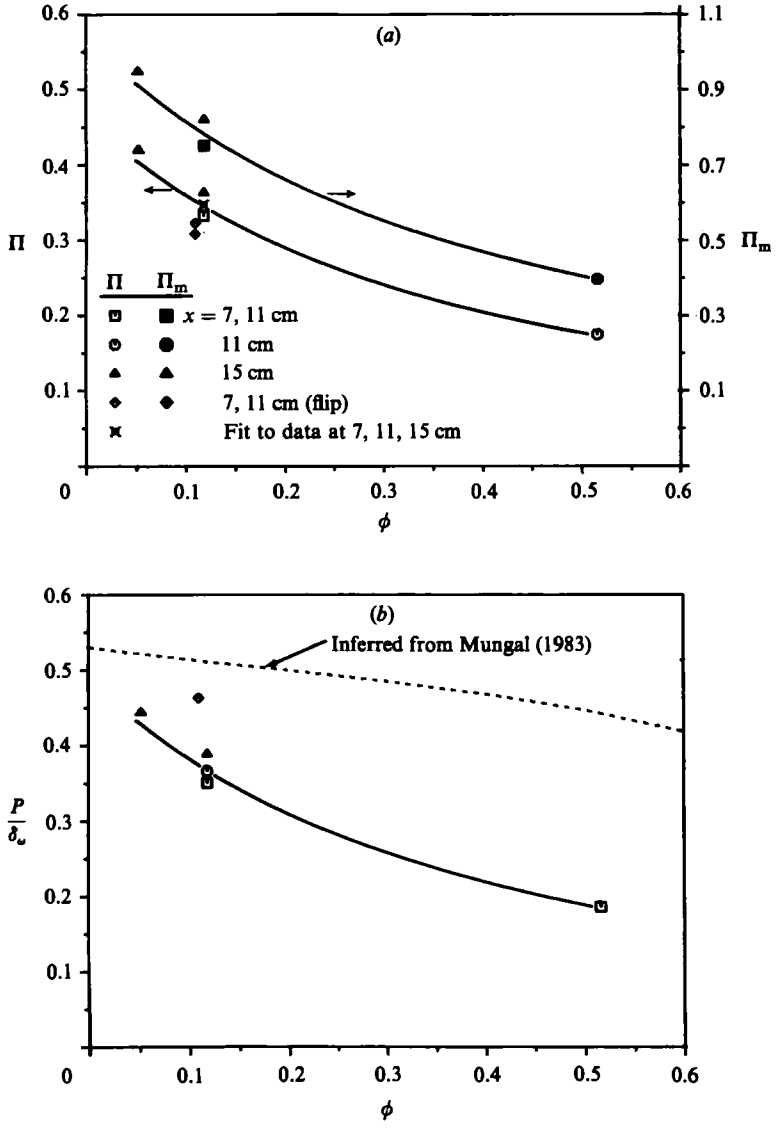

FIGURE 21. (*a*) Conversion efficiencies Π and Π_m, and (*b*) product thickness, P/δ_ω, as functions of overall lean-to-rich reactant ratio. ▫, $x = 7$, 11 cm; ○, best fit to data ($x = 7$, 11, 15 cm); △, $x = 15$ cm; ◇, $x = 7$, 11 cm (flip).

(1981) to assess the extent of reaction in a liquid mixing layer, may be obtained from Π:

$$\frac{P}{\delta_\omega} = \frac{V_{O_3}\Pi(|\delta_h - \delta_\ell|)}{\delta_\omega}.$$

Also of interest is the fraction of the O_3 in the layer, mixed on the molecular level, that has undergone chemical reaction Π_m:

$$\Pi_m \equiv \frac{\Pi V_{O_3}}{V_{O_3} - \Delta V_{O_3}} = \frac{\Pi}{FM},$$

where

$$\Delta V_{O_3} \equiv \frac{1}{|\delta_h - \delta_\ell|}\int_{\delta_\ell}^{\delta_h} P_{O_3}(\eta')\,d\eta'$$

and $P_{O_3}(\eta')$ is the local probability of finding pure unmixed O_3-bearing free-stream fluid. The conversion fractions, Π and Π_m, and product thickness are plotted as functions of ϕ for both the non-flip and flip experiments in figure 21. The data show that as the NO mole fraction in the free stream is increased from 2 to 20 times stoichiometric proportions, i.e. as ϕ decreases from 0.5 to 0.05, the fractional conversion of lean reactant and the product thickness increase. Figure 21 (*a*) shows that, while the fraction of O_3 mixed on the molecular level that has reacted exceeds the fraction of entrained O_3 that has reacted, Π_m generally is less than one, indicating the presence of mixed but unreacted lean reactant. The data also show that switching the lean reactant from the low-speed to the high-speed stream does not alter Π, but does produce a significant decrease in Π_m and a substantial increase in P/δ_ω. Hence, it appears that while the amount of product formed increases in the flip experiment owing to the entrainment asymmetry, a smaller fraction of mixed high-speed lean reactant undergoes reaction, owing to lower reaction rates.

The dependence of P/δ_ω on ϕ, inferred from the post-mixing transition data of Mungal (1983), is also shown in figure 21 (*b*). While the data from both studies indicate that the amount of product formed increases as the rich-reactant concentration is increased, some significant differences exist between the two sets of results. In the present experiments, P/δ_ω is much lower than in Mungal's experiments, but more than doubles over the range of ϕ investigated. Mungals' data show a modest 15% increase in product thickness. While changes in entrainment and mixing dynamics of the layer, which occur during the mixing transition, may contribute to these differences, there is evidence that the effects of finite-rate chemistry play a role in determining the structure of the layer in the present study, while fast-chemistry conditions prevail in the H_2–F_2 experiments.

The characteristic chemical times in the present experiments may be estimated from

$$\tau_c \equiv 1/k(\mathrm{NO})_\infty, \tag{6.3}$$

where the subscript ∞ indicates free-stream conditions. Substituting the sum of the rate coefficients for reactions (3.1*a*) and (3.1*b*) for k, and the experimental values of $(\mathrm{NO})_\infty$ into (6.3) yields,

$$128\ \mu\mathrm{s} < \tau_c < 1220\ \mu\mathrm{s}.$$

Mungal estimates that a typical chemical time in his experiments is approximately 2 μs. The Damköhler number Da defined as

$$Da \equiv \frac{\tau_m}{\tau_c} = \frac{\text{characteristic mixing time}}{\text{characteristic chemical time}},$$

can be calculated if a characteristic mixing time can be determined. By this definition, $Da \ll 1$ implies frozen chemistry and $Da \gg 1$ implies fast chemistry. Broadwell & Breidenthal (1982) suggest that two timescales bracket the mixing times in boundary-free mixing zones. The two timescales are the eddy-turnover, or cascade time,

$$\tau_\delta \approx \delta_\omega/\Delta U,$$

and the small-scale diffusion time,

$$\tau_{\lambda_0} \approx \tau_\delta Sc\, Re_\delta^{-\frac{1}{2}},$$

which is the time required to diffuse across the Kolmogorov scale. Under the present conditions of $Sc \approx 1$ and $Re \approx 1000$–2000, $\tau_\delta/\tau_{\lambda_0} > 30$, suggesting that the rate-limiting mixing step is characterized by τ_δ. Taking

$$Da = \tau_\delta/\tau_c, \tag{6.4}$$

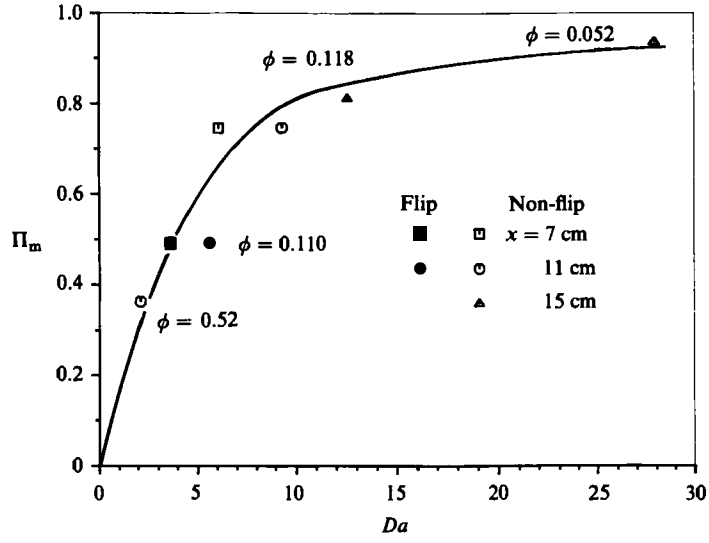

FIGURE 22. Conversion efficiency Π_m as a function of large-scale Damköhler number, equation (6.4).

then $$2 < Da < 28$$

in the present investigation, while

$$Da \approx 10^3$$

in Mungal's study.

For frozen chemistry ($Da \ll 1$), reactants may coexist in space since reaction proceeds too slowly to deplete mixed reactants. For fixed ϕ, as reaction rates increase, more mixed reactant will be consumed, resulting in a reduction of mixed fluid and an increase in the amount of product in the layer. Hence, conversion fractions are expected to increase as Da increases from 0, ultimately attaining complete conversion of mixed lean reactant at the fast-chemistry limit. The experimental data, figure 22, show the expected trends and indicate that data from both flip and non-flip experiments are consistent when variations in Damköhler number are considered.

6.3. *Fast-chemistry predictions*

The fast-chemistry formalism provides a simplified procedure for prediction of the properties of turbulent reacting flows (Bilger 1980). A semi-empirical technique can be used to obtain estimates of the mean normalized product mole fraction $\bar{\zeta}$ that would exist in the present mixing layer if the rate of the NO–O_3 was infinite, $Da \to \infty$. At the fast-chemistry limit, $\bar{\zeta}$ can be determined by weighting and integrating the p.d.f.s of the mixture fraction (Masutani 1985). Since the hydrodynamic conditions in the non-reacting and reacting mixing layers were identical, the statistics of the non-reacting O_3 mole fraction, $\xi(x, t)$, should be identical with those of the mixture fraction in the reacting flow. Hence, the experimentally determined p.d.f.s of $\xi(x, t)$ were used to predict the fast-chemistry mean values of NO_2 concentration.

The fast-chemistry predictions of $\bar{\zeta}$ are compared with the measured $\bar{\zeta}$ in figure 23. The fast-chemistry predictions overestimate the amount of product formed in the mixing layer for all of the experiments. A portion of this excess may be attributed

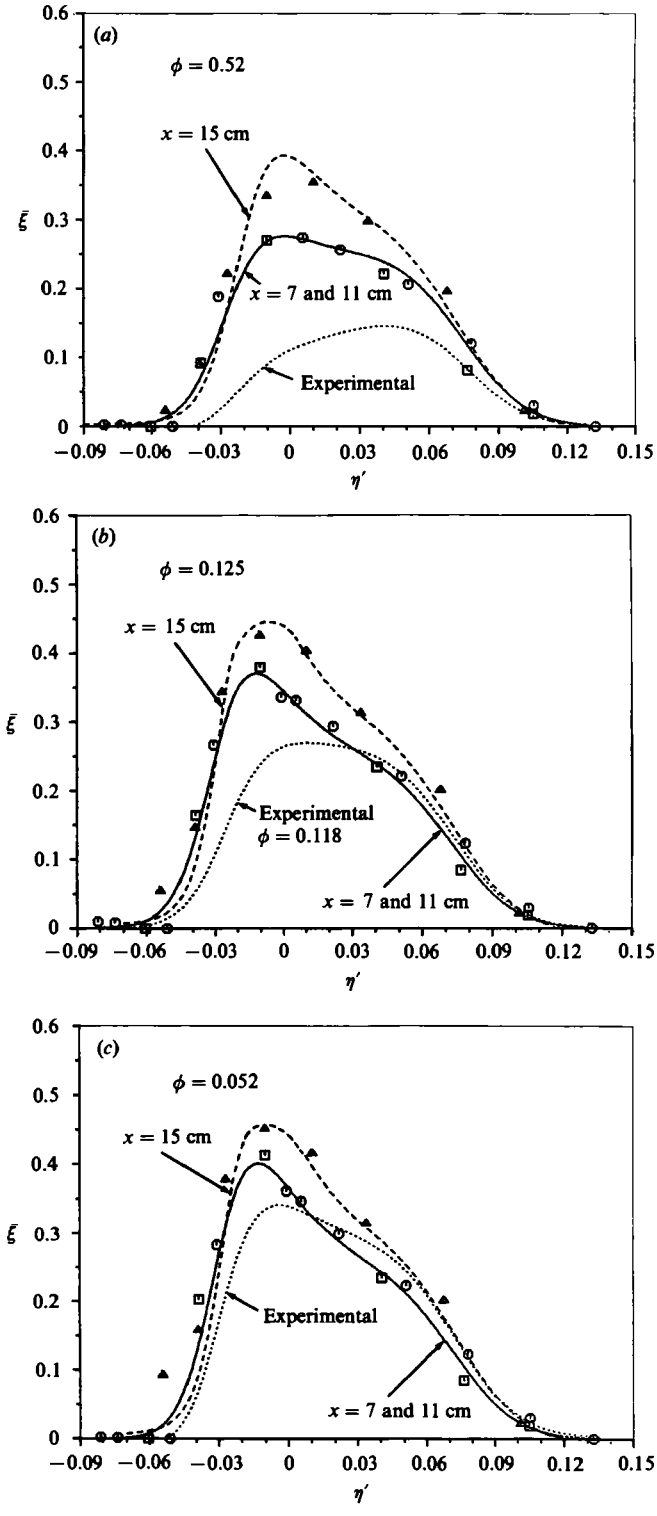

FIGURE 23. Comparison of fast-chemistry predictions of mean normalized product profiles with experimental results for three reactant ratios. ⊡, $x = 7$ cm; ⊙, 11 cm; △, 15 cm.

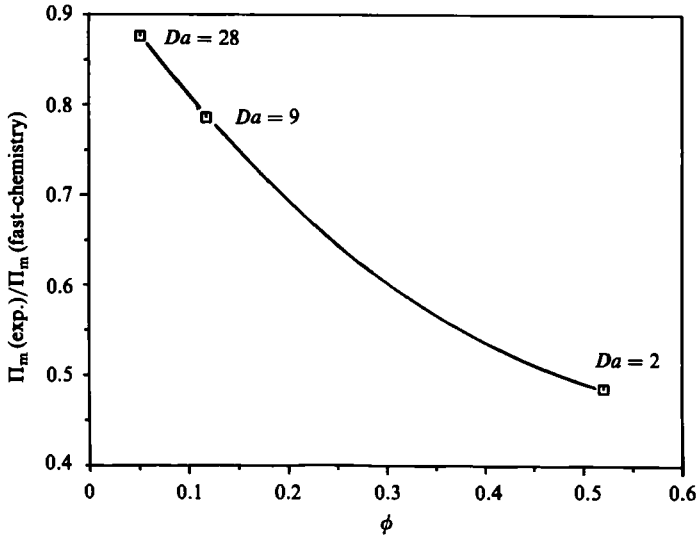

FIGURE 24. Comparison of fast-chemistry predictions of conversion efficiency with experimental results. *Da* is the large-scale Damköhler number, equation (6.4).

to overestimates of mixed fluid due to the finite spatial resolution of the concentration probe. The predictions indicate an increase in product for $x > 11$ cm, as a consequence of the streamwise evolution of ξ_p, which is not detected in the experiments. The predicted profiles of $\bar{\zeta}$ are more strongly skewed toward the lean-reactant-bearing free stream than are the data. The discrepancies between the data and the fast-chemistry predictions decrease as ϕ decreases (i.e. as the NO free-stream concentration and Damköhler number increase).

To quantify the degree to which the fast-chemistry model overpredicts the amount of product formed, ratios of the measured-to-calculated conversion fraction Π_m are plotted in figure 24. Also shown in this figure are the corresponding values of *Da*, equation (6.4). As *Da* increases, the measured Π_m approaches the fast-chemistry predictions.

7. Observations on the reacting mixing layer

The results of the reacting flow experiments show that the structure of the chemically reacting mixing layer is influenced by the asymmetric entrainment and mixing characteristics of the flow and by finite-rate reaction kinetics.

The measured mean normalized product distributions $\bar{\zeta}$, as well as the fast-chemistry predictions of $\bar{\zeta}$, exhibit a skewness toward the free stream containing the lean reactant, which becomes more pronounced as the rich-reactant concentration increases. Mungal (1983) proposed that this effect was due to enhanced reaction occurring at the boundaries of the homogeneous core regions nearest the lean-reactant-bearing free stream as fresh reactant is drawn in and mixed directly with core fluid by the action of secondary streamwise vortices. While the results of the present study suggest a strongly two-dimensional flow field, they do not discount the possibility that secondary vortices, or smaller-scale 'nibbling' activity could be responsible for this type of locally augmented chemistry. However, the displacement of the peak values of the mean product (or temperature) distributions with changing stoichiometry resembles the physical displacement of the reaction sheets with

increasing rich-reactant concentration, which is assumed to occur at the fast-chemistry limit. This similarity suggests a simple alternative explanation for the observed skewed profiles. As the free-stream NO increases above stoichiometric proportions, the reaction sheets (for fast chemistry) or reaction zones (for finite-rate chemistry) will shift toward those locations where reactants are mixed at stoichiometric proportions, i.e. closer to the unmixed lean-reactant interface. Product-species concentrations are highest in these sheets or zones, and will be reduced by dilution as these scalars are subsequently convected away. A stationary probe therefore will detect, on average, higher product concentrations nearer the boundary adjacent to the lean-reactant-bearing free stream.

Switching the lean reactant from the low-speed to the high-speed stream increased the amount of product formed, for fixed global stoichiometry, but the increase was accompanied by a reduction in the conversion fraction Π_m. A fast-chemistry model will not account for the observed reduction in conversion fraction. Hence, in the flip experiment, the mixing-layer structure is influenced both by the entrainment and mixing asymmetry, which increases the volume of mixed lean reactant in the layer, and by finite-rate chemistry, which increases the probability of detecting mixed but unreacted volumes of the lean reactant.

The present experiments appear to span a range of conditions over which reaction kinetics vary from finite-rate to fast chemistry. The data, taken in conjunction with the earlier studies of Shea (1976) and Mungal (1983), suggest a tentative criterion for fast-chemistry conditions in the mixing layer, which is based on a Damköhler number expressed in terms of the large-scale mixing time τ_δ. The results of these experiments suggest that gaseous reacting mixing layers approach fast-chemistry conditions for $Da > 10$.

The experimental data, figures 16 and 17, indicate that in reacting flows there is an apparent depletion of 'unmixed' reactants. Assuming that the interfacial diffusion zones are regions of chemical activity, an explanation for this observation may be proposed. Chemical reaction serves as a 'sink' for reactants, which can produce an increase in the concentration gradients in the vicinity of reaction zones in non-premixed systems. This effect is well known in modelling studies of laminar non-premixed flames (Williams 1985). The increased gradient will result in enhanced diffusive transport of reactants in the vicinity of reaction zones, resulting in the measurement of an apparent depletion of 'unmixed' reactants by a probe with finite spatial resolution.

8. Summary and conclusions

The present experimental investigation examined the structure of a non-reacting and reacting, constant-density, plane mixing layer in a flow regime prior to the onset of the mixing transition.

Temporally and spatially resolved measurements of velocity and the concentrations of a conserved scalar and of a reactant and a product species were obtained at streamwise locations ranging from 205 to 738 initial boundary-layer thicknesses of the mixing layer downstream of the trailing edge of the splitter plate.

Data on the statistics of a conserved scalar in the non-reacting mixing layer indicate that significant quantities of molecularly mixed fluid exists in this flow regime. In contrast, Koochesfahani (1984) detected very little mixed fluid in a liquid plane mixing layer at a similar value of Re_δ. This difference emphasizes the

importance of molecular diffusion in determining the concentration structure of the gaseous mixing layer in this flow regime.

In the layer, mixed fluid exists in finite-thickness, interfacial diffusion zones which border parcels of unmixed fluid and in regions of nearly homogeneous composition. At a fixed streamwise location, the composition of the homogeneous zones assumes a preferred value of the mixture fraction ξ_p. The value of ξ_p is invariant across the layer, but does increase downstream, suggesting that the mixing layer is evolving over the range of x studied. There is evidence that this evolution reflects an initial, large asymmetry in the entrainment of high-speed fluid in the layer which relaxes slowly to an asymptotic state, in which ξ_p is determined by the mean entrainment rates of free-stream fluid into the layer. The observed invariance of ξ_p across the layer has not been reproduced in numerical simulations of the mixture fraction p.d.f. The calculated p.d.f.s exhibit a mixed-fluid peak ξ_p, which varies continuously across the mixing region (Pope 1980; Kollman & Janicka 1982; Givi 1984). Hence, further refinements to the modelled terms in the p.d.f. transport equations are required.

In previous investigations (Konrad 1976; Koochesfahani 1984) a marked asymmetry in the quasi-steady rates of entrainment and mixing of fluid from the two feed streams has been observed in which the mixing layer ingests and mixes larger volumes of high-speed fluid. This study indicates that, for the present conditions, the layer entrains and subsequently mixes high-speed fluid at approximately twice the rate of low-speed fluid.

Reacting flow experiments were conducted in which the concentration of a reactant species, O_3, and a product species, NO_2, were obtained simultaneously. In three of these experiments, the lean reactant, O_3, was introduced into the low-speed stream. A fourth 'flip' experiment was performed, in which O_3 was switched into the high-speed stream, to determine the effects of the asymmetric entrainment and mixing characteristics of the layer on the concentration structure of the reacting flow.

A marked increase in the amount of product formed in the mixing region was observed as the free-stream concentration of NO was increased from 2 to 20 times stoichiometric proportions. For a fixed value of overall reactant ratio ϕ, switching the lean reactant from the low-speed to the high-speed stream resulted in an increase in the total amount of product (NO_2) formed, but a decrease in the fraction of mixed lean reactant that had undergone chemical reaction.

Comparison of the data with the predictions of a semi-empirical fast-chemistry model and with the experimental results of Mungal (1983) suggests that the variations in concentration structure observed in the present experiments arise from a combination of factors, including asymmetric entrainment and mixing characteristics of the flow and effects of finite-rate chemistry.

A Damköhler number, based on large-scale mixing times, is proposed to describe gas-phase, reacting mixing zones. This parameter may be used to determine the applicability of a fast-chemistry analysis to a particular reacting flow situation. For this definition of Da, the present experiments fall within the range $2 < Da < 28$. A tentative 'threshold' for fast-chemistry conditions is $Da > 10$.

The authors thank G. Kychakoff, R. Howe and R. A. Booman for assistance with the PLIF measurements of NO and B. J. Cantwell for helpful discussion. Financial support for this work was provided in part by the Air Force Office of Scientific Research.

REFERENCES

ALBER, I. E. & BATT, R. G. 1976 Diffusion-limited chemical reactions in a turbulent shear layer. *AIAA J.* **14**, 70.

BATES, S. C. 1977 Luminescent visualization of molecular and turbulent transport in a plane shear layer. *MIT Gas Turbine Lab. Rep.* 134.

BATT, R. G. 1977 Turbulent mixing of passive and chemically reacting species in a low-speed layer. *J. Fluid Mech.* **82**, 53.

BILGER, R. W. 1980 Turbulent flows with non-premixed reactants. In *Turbulent Reacting Flows*, p. 65. Springer.

BREIDENTHAL, R. E. 1981 Structure in turbulent mixing layers and wakes using a chemical reaction. *J. Fluid Mech.* **109**, 1.

BROADWELL, J. E. & BREIDENTHAL, R. E. 1982 A simple model of mixing and chemical reaction in a turbulent shear layer. *J. Fluid Mech.* **125**, 397.

BROWAND, F. K. & LATIGO, B. O. 1979 Growth of the two-dimensional mixing layer from a turbulent and non-turbulent boundary layer. *Phys. Fluids* **22**, 1011.

BROWN, G. L. & ROSHKO, A. 1974 On density effects and large structure in turbulent mixing layers. *J. Fluid Mech.* **64**, 775.

COLES, D. 1981 Prospects for useful research on coherent structure in turbulent shear flow. *Proc. Indian Acad. Sci.* **4**, 111.

CORCOS, G. M. & SHERMAN, F. S. 1976 Vorticity concentration and the dynamics of unstable free shear layers. *J. Fluid Mech.* **73**, 241.

DIMOTAKIS, P. E. 1984 Entrainment into a fully developed two-dimensional shear layer. *AIAA Paper No.* 84-0368.

DRISCOLL, J. F., SCHEFER, R. W. & DIBBLE, R. W. 1982 Mass fluxes $\rho'u'$ and $\rho'v'$ measured in a turbulent non-premixed flame. In *Proc. 19th Symp. on Combustion*, p. 477, The Combustion Institute.

GIVI, P. 1984 Turbulent reacting flows. Ph.D. thesis, Carnegie-Mellon University.

JIMENEZ, J., MARTINEZ-VAL, R. & REBOLLO, M. 1979 The spectrum of large-scale structures in a mixing layer. In *Proc. 2nd Symp. on Turbulent Shear Flows, Imperial College.*

KOLLMANN, W. & JANICKA, J. 1982 The probability density function of a passive scalar in turbulent shear flows. *Phys. Fluids* **25**, 1755.

KONRAD, J. H. 1976 An experimental investigation of mixing in two-dimensional turbulent shear flows with applications to diffusion-limited chemical reactions. *Project SQUID Tech. Rep.* CIT-8-PU.

KOOCHESFAHANI, M. M. 1984 Experiments on turbulent mixing and chemical reactions in a liquid mixing layer. Ph.D. thesis, California Institute of Technology.

KOOCHESFAHANI, M. M. & DIMOTAKIS, P. E. 1984 Laser induced fluorescence measurements of concentration in a plane mixing layer. *AIAA Paper No.* 84-0198.

KYCHAKOFF, G., HOWE, R. D. & HANSON, R. K. 1984 Quantitative flow visualization technique for measurements in combustion gases. *Appl. Opt.* **23**, 704.

LASHERAS, J. C., CHO, J. E. & MAXWORTHY, T. 1986 On the origin and evolution of streamwise vortical structures in a plane, free shear layer. *J. Fluid Mech.* **172**, 231–258.

MASUTANI, S. M. 1985 An experimental investigation of mixing and chemical reaction in a plane mixing layer. Ph.D. thesis, Stanford University.

MASUTANI, S. M. & BOWMAN, C. T. 1982 A fiberoptic absorption probe for measurement of a conserved scalar in nonpremixed turbulent reacting flow. *Western States Section Combustion Institute Meeting, October 1982, Paper* 82-62.

MUNGAL, M. G. 1983 Experiments on mixing and combustion with low heat release in a turbulent shear flow. Ph.D. thesis, California Institute of Technology.

POPE, S. B. 1981 Calculation of a turbulent mixing layer involving the $NO+O_3$ reaction. In S. V. Sherikar & R. Chevray, *Proc. 3rd Symp. on Turbulent Shear Flows, University of California.*

ROSHKO, A. 1976 Structure of turbulent shear flows: a new look. *AIAA J.* **14**, 1349.

SHEA, J. R. 1977 A chemical reaction in a turbulent jet. *J. Fluid Mech.* **81**, 317.

SHERIKAR, S. V. & CHEVRAY, R. 1981 A chemically reacting plane mixing layer. In *Proc. 3rd Symp. on Turbulent Shear Flows, University of California.*

WALLACE, A. K. 1981 Experimental investigation of the effects of chemical heat release in the reacting turbulent plane shear layer. Ph.D. thesis, University of Adelaide.

WILLIAMS, F. A. 1985 *Combustion Theory.* Benjamin/Cummings.

WINANT, C. D. & BROWAND, F. K. 1974 Vortex pairing: the mechanism of turbulent mixing layer growth at moderate Reynolds number. *J. Fluid Mech.* **63**, 237.